Using Virtual Life Management® (VLM®) to Predict the Fatigue Response of a Simple Laboratory Specimen

Robert Tryon
Chief Technology Officer
Vextec Corporation
Brentwood, Tennessee, USA

Abstract

A Monte Carlo analysis method combining the models of dislocation theory with random variable statistics is used to predict the fatigue response scatter due to the random nature of the physical microstructure. The microstructure is modeled using the appropriate statistical distributions for high strength materials typical of those used in propulsion structures. The method simulates crack growth through the random microstructure using the appropriate fracture mechanics processes. The method allows for three stages of damage accumulation and simulates the transition from one stage to the next using the proper mechanistic linkages. The method is general and considers the entire range of damage accumulation sequences; from crack nucleation of the initially unflawed structure to final fast fracture

1 Introduction

This paper gives an example of how probabilistic methods can be used to predict the variability expected in the fatigue test of simple laboratory specimens such as smooth round bars. The variability observed in laboratory experiments is discussed. The physical source of the variability is identified. Fracture mechanics based models that account for the physical mechanism occurring during fatigue are introduced. Using these models, the governing material parameters likely to have significant uncertainty are identified and the uncertainty is quantified. A Monte Carlo simulation routine is developed using the mechanistic model and the governing random variables to predict the scatter in the smooth bar response. For the purpose of this paper, fatigue is defined as the entire range of damage accumulation sequences; from crack nucleation of the initially unflawed bar to final fast fracture.

2 Background

2.1 Various Stages of Fatigue

Current fatigue life prediction methods in metallic components consider three stages: crack initiation, long crack propagation and final fracture. Long crack propagation and final fracture are the stages of damage accumulation that are well characterized using linear elastic or elastic-plastic fracture mechanics. Crack initiation is the early stage of damage accumulation where small cracks (cracks with depths less than several grain diameters) have been observed to deviate significantly from predicted long crack fracture mechanics behavior [1]. The deviation is attributed to the heterogeneous media in which small cracks evolve [2].

The crack initiation stage can be broken down into two phases: crack nucleation and small crack growth. Crack nucleation is the locally complex process of crack formation on the microstructural scale. Crack nucleation is characterized by smooth fracture surfaces at angles inclined to the loading direction. This type of failure is indicative of shear stress Mode II (sliding mode) fracture. Although loading has been shown to effect the nucleation size [3,4], experimental evidence suggest that the nucleation size is on the order of the grain size [5,6,7].

Small crack growth is characterized by fracture surface striations perpendicular to the loading direction. This type of failure is indicative of tensile stress Mode I (opening mode) fracture. The behavior of small cracks tends to transition to linear or elastic-plastic fracture mechanics behavior when the crack depth reaches about ten mean grain diameters [8]. Crack nucleation and small crack growth must be modeled separately because different mechanisms control each phase. The relative importance of the crack nucleation stage on overall fatigue life depends on several factors. Materials which exhibit a strong preference for planar slip show a strong correlation between the crack causing final fracture and the earliest nucleated cracks [9]. Materials which prefer cross slip showed almost no correlation between the crack causing final fracture and the earliest nucleated cracks [9]. The relative importance of

the crack nucleation may also depend on the loading condition. If the loading is relatively low (high cycle fatigue), the majority of life will be spent in the nucleation of a crack. If the loading is high (low cycle fatigue), cracks may nucleate early and spend the remainder of the fatigue life in the crack growth stages. However, high strength materials have been shown to spend the majority of fatigue life in the crack nucleation stage, even during low cycle fatigue [10].

2.2 Scatter in Fatigue Life

The coefficient of variation (COV) of fatigue life tests range widely depending on the material alloy and load level. Even for well controlled laboratory test of annealed smooth specimens at room temperature, the COV varies from less than 10% [9] to over 500 % [11] for different steel alloys. This indicates that the fatigue reliability experienced by components in the field may be substantially attributed to the material behavior.

Sasaki *et al.* [9] compare the variation in crack nucleation life of mild steel, pure copper, and stainless steel. They found that the COV clearly depends on the stacking fault energy denoted by γ. Relatively low COV was found for mild steel, which has high γ (wavy slip), and high COV was found for stainless steel, which has low γ (planar slip). Copper, which has an intermediate γ, was found to have a value of the COV between mild and stainless steel.

Figure 1 shows the relative scatter in the different stages of crack growth for sixteen mild steel specimens exposed to high cycle fatigue [12]. The specimens were shallow notched and tested in rotating bending. The cracks nucleated at a size roughly equal to the mean grain size (0.07 mm). The small crack regime for this data extends from the initiation event until the crack reaches about eight times the mean grain size (0.6 mm). The long crack growth regime extends from 0.6 mm to failure. Figure 1 illustrates the larger amount of scatter in the early stages of crack growth with relatively little scatter (similar slopes) in the large crack growth stage. The variation is attributed to the heterogeneous media in which small cracks evolve.

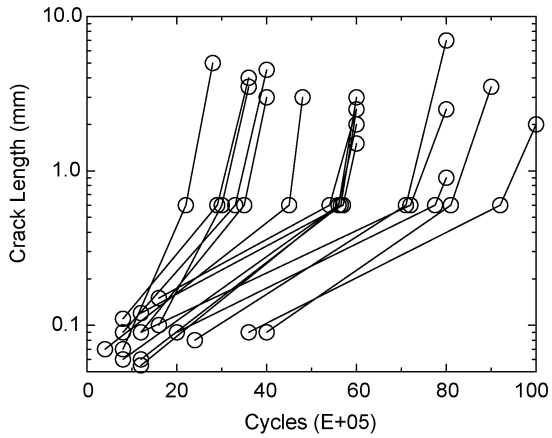

Figure 1: Crack growth curves for mild steel emphasizing the large scatter in the early stages.

Table 1 shows the scatter factors for a NiCrMoV steel turbine rotor shaft material data [13]. The specimens were shallow notched round bars tested in rotating bending low cycle fatigue. The scatter factors are for a 99.87 % (-3 σ) reliability at 90 % confidence level using the life reduction model found in Fu-Ze [14], which assumes a lognormal life distribution. The behavior in Figure 1 and Table 1 is observed for different stresses amplitudes and materials [9,12,15,16].

Table 1: Scatter factors for stainless steel in low cycle fatigue.

Failure definition	Number of samples	Mean life (cycles)	Scatter factor	-3 σ life (cycles)
Nucleation	36	26,700	44.2	604
Small crack	36	52,400	15.5	3380
Final fracture	14	82,400	2.78	29,600

The values in Table 1 show the importance of material response scatter. The scatter factors are life reduction factors for material response scatter only. They do not account for variations in loading, geometry, environment, temperature or size effect. The potential for improved design through the reduction of material scatter is great. When you consider that fatigue is estimated to account for at least 90 % of all service failures due to mechanical causes [17], understanding the statistical aspects of fatigue becomes paramount.

Limited experimental work has been performed with regard to the effect of microstructural variation on other aspects of material response. Gokhale and Rhimes [18] prepared pure aluminum to give several grain size

distributions with the same mean grain size but different variances. They found that the scatter in grain size played a primary role in controlling yield stress, ultimate tensile stress, reduction in area and the area under the stress-strain curve. The parameters were much more sensitive to changes in the grain size variance than to changes in the mean grain size. Their research emphasizes the importance of microstructural variation with regard to any type of plastic behavior which is likely to be important to crack initiation and growth kinetics.

2.3 Probabilistic Micromechanics

Most crack nucleation models are empirically based macrostructural models [19]. They reduce crack nucleation to simple parametric functions of macro-stress and macro-strain variables. As such, the macrostructural models assume the material to be homogeneous and isotropic. The models are necessarily approximate because they cannot represent the heterogeneous media in which the damage processes occur. In contrast to macrostructural models, micromechanical models establish material behavior based on the explicit response of the microelements, such as dislocations and slip planes. Micromechanics have successfully explained the qualitative behavior of crack initiation. However, a theoretical crack initiation model which explicitly relates the microstructure to the macroresponse has not been developed because too many complex micromechanical processes are operating simultaneously [20].

Statistical concepts have been used to develop empirical fatigue life models in which the independent variable (applied stress or strain) is considered deterministic and the dependent variable (life) is considered random [21]. The models do not account for the mechanisms that regulate fatigue damage and thus, the source of the scatter is unknown and must be attributed to incomplete data and missing parameters. The models cannot be used to accurately describe materials and loading conditions that are not explicitly part of the data-based test program.

This study addresses the statistical aspects of fatigue using a fundamentally different approach. The fatigue mechanisms are considered and the independent variables, which include material variables that govern response, are recognized as random variables. The approach identifies the sources of uncertainty and quantitatively links the variation in the material microstructure to the scatter in the fatigue response.

The research is based on the concepts of probabilistic mesomechanics [22] which provides the relationships between the microstructural material properties and non-continuum mechanics [23]. In this research, the mesoelements are defined as the individual grains of a polycrystalline aggregate. Each grain is considered a single crystal with homogeneous (although not isotropic) properties. The properties are considered to vary from grain to grain. The macrostructure is modeled as an ensemble of grains. The material properties of the ensemble of grains are defined using the appropriate statistical distributions. Mesomechanical modeling is an approximation of the actual material because certain properties will vary within a grain. However, it is believed that mesomechanics is a better approximation of the true material characteristics than macromechanics.

Mesomechanics also recognizes the multiple stages of fatigue damage accumulation such as crack nucleation, small crack growth and long crack growth. Each stage is driven by different mechanisms and must be distinctly modeled. The stages must be quantitatively linked because the crack grows successively from one stage to the next. In this research, a theoretical micromechanical model is used to determine the number of cycles necessary to nucleate a crack in the individual grains. A combination of models based on empirical observations and theoretical micromechanics are used to determine the number of cycles necessary to grow the cracks from nucleation to the long crack regime. An empirically based (Paris law) model is used to determine the number of cycles necessary for the crack to grow through the long crack regime to the critical crack size. Failure of the macrostructure is defined by the first crack to nucleate and grow beyond the critical crack size. The statistical distribution of fatigue life for the macrostructure is determined using Monte Carlo simulation methods. The probabilistic mesomechanical model provides a direct quantitative link between the variations in the material microstructure to the scatter in the fatigue behavior.

Many material and structural design factors influence component reliability in terms of the defined durability problems. From a material performance standpoint, many of these factors are at work in the durability “size effect”. The size effect was first reported by Peterson [24] when he noticed that the mean fatigue life and variation in fatigue life were a function of the stressed area. The size effect has a fundamental role in controlling reliability because damage accumulation starts on a small scale and grows through various characteristic sizes, each with its own geometric complexities, constitutive laws, and heterogeneities. Fatigue behavior cannot be fully understood and predicted without obtaining information about each of the characteristic sizes, or what can be called mesodomains [23]. Nested models can link each of the mesodomains to determine the response of the macrodomain [25].

The concepts of mesomechanics can be used to explicitly examine each of the characteristic sizes or

mesodomains. For example, a fleet of simple polycrystalline metallic components may be divided into six mesodomains as shown in Table 2. At each level, heterogeneities can be introduced from various sources and fatigue damage can accumulate via various mechanisms.

Table 2: Mesodomains of a mechanical component

Mesodomain	Sources of variation	Damage accumulation mechanisms
dislocation level	vacancies, interstitials	dislocation pile-up
sub-grain level	slip bands, micro-voids, second phase particles	slip band decohesion
grain level	crystallographic orientation, twins, inclusions	crack nucleation
specimen level	surface finish, cracks, notches	small crack growth
component level	cracks, notches, processing, geometry, machining	large crack growth
fleet level	heat treatment, service duty, applications	NDE inspection screening, life distributions

The true primary mesodomain is below the dislocation level. The most primitive variables controlling fatigue may be at the atomic level. Modeling at such levels is not yet possible and is not required for the purposes of the present study. The slip process, which takes place on slip steps typically 0.1 μm wide, is of continuum scale with respect to the atomic size of 0.5 *nm* [26]. The smallest practical mesodomain depends on the material, loading and available information gathering techniques. The research has focused on the use of slip band models from the sub-grain mesodomain, together with probabilistic variables being defined at the grain size mesodomain. These models are used to predict behavior for the specimen mesodomain.

The specimen level is an artificial mesodomain because there are no specimens in the fleet. Specimens are generally prepared to limit the introduction of heterogeneities. However, the bulk of the information used in design is usually gathered from specimen testing, so it is important to understand the characteristics of this level. Specimen testing can identify scale effects, defect origins, and processing influences on crack initiation.

A large component such as an aeroengine fan blade will have several mesodomains between the grain size and the component level. The airfoil and the dovetail would be two component—scale mesodomains. Properties such as the grain size, material properties, and surface finish are different in these two mesodomains. The delineation of the mesodomains is specific to the material, geometry, loading and failure mode.

The overall fatigue response at the fleet level is predicted by nesting the individual mesoscale models. The lowest level model uses the appropriate mesoscale parameters to determine the initial state of the next level. This level uses the results from the previous level along with the appropriate parameters to determine the initial state of the next level and so on. Through the use of nested models, fleet reliability can be linked to the heterogeneities at each mesodomain. Additionally, by modeling each level of the fatigue process individually, and rigorously linking the levels, various size effects are included.

3 Damage Accumulation Models

3.1 Overview of a Probabilistic Microstructural Fatigue Model

The probabilistic fatigue modeling algorithm discussed in this chapter concentrates on the regimes in which the effects of the local variation in the microstructure are assumed dominant. The purpose of the algorithm is to assess only the microstructural effects. Variations in the applied loading and global geometry are not considered. The fatigue process is divided into three phases. The first phase is the crack nucleation phase in which damage accumulates to form a crack in an initially uncracked structure. The second phase is the small crack growth phase in which the crack size is on the order of the microstructure. The third phase is the long crack growth phase in which the crack size is large compared to the microstructure.

The algorithm uses microstructural models that predict crack nucleation life and crack nucleation size which have been proposed in the literature. These models predict damage accumulation through irreversible dislocation

pile-up at microstructural obstacles. Cracks nucleate when the critical strain energy is exceeded.

Although the material fatigue response algorithm is able to model each of the crack nucleation mechanisms described above, of particular interest to initially undamaged components is the slip band cracking within the grain. Many of the high strength materials currently used in safety critical structures accumulate damage through the creation of persistent slip bands. The theory of continuously distributed dislocations is used to model the persistent slip band within a grain. Dislocations pile up at the grain boundaries with each load cycle. When the energy associated with the dislocation pile-up, exceed a critical value, a crack forms along the slip band the size of the metallic microstructural grain.

The second phase is the small crack growth phase in which the crack size is on the order of the microstructure. The crack growth rate is modeled as a function of the crack tip opening displacement (CTOD). The theory of continuously distributed dislocations is used to model the CTOD. The plastic zone is modeled as dislocations distributed ahead of the crack tip. The tip of the plastic zone is either propagating freely within a grain or blocked at the grain boundary. The CTOD depended on the relative location of the crack tip and the plastic zone tip. The crack grows in the small crack growth phase until the plastic zone spanned many grains so that local microstructural variations have little effect.

The third phase is the long crack growth phase. The crack growth rate is modeled using Paris law. The microstructural variations are not explicitly considered. All variation in long crack growth is model by allowing the Paris law coefficient to be a random variable.

Fatigue test of an ensemble of smooth round bar (SRB) specimens is used to show the capabilities of the method. The overall fatigue response of the SRB is predicted by nesting the individual mesoscale models. The crack nucleation model uses the appropriate mesoscale parameters to determine the initial state of the small crack growth model. This model uses the results from the previous crack nucleation model along with the appropriate parameters to determine the initial state of the long crack growth model. Using nested models, specimen reliability can be linked to the heterogeneities at each mesodomain. Additionally, by modeling each level of the fatigue process individually, and rigorously linking the levels, various size effects are included.

The local microstructural variables considered random in this chapter are: grain size, grain orientation, micro-stress, and the frictional stress needed to move dislocations. The grain size statistical distribution is determined from data in the literature. The grain orientation statistical distribution is determined for both surface and interior grains using theoretical considerations. The micro-stress statistical distribution is determined from a Voronoi cell finite element model [27]. The variables are common to both the crack nucleation and small crack growth models. The grain shape is assumed equiaxial and the grain orientation is untextured and described using the face-center-cubic slip system. The loading and material properties within a grain are homogeneous although not isotropic. The material properties vary from grain to grain.

3.2 Crack Nucleation

3.2.1 *Micromechanics of Crack Nucleation*

Fatigue crack nucleation is a complex and obscure process. The mechanisms for crack nucleation change with material, loading, temperature and environment. One overriding observation is that cracks tend to nucleate near the free surface. For many loading conditions, the highest loads are at the surface. However, even when the nominal stress is constant throughout, cracks tend to nucleate at the surface because deformation of each grain is allowed to concentrate on a preferred crystallographic plane. In the interior, deformation on a single crystallographic plane is hampered by the constraints of the surrounding grains.

Experimental evidence clearly shows that defects in the material can cause fatigue crack nucleation by acting as stress concentrations and the cracks tend to nucleate along the preferred slip plane [28]. Examples of defects include surface pores, ceramics inclusions, second phase particles and microcracks. The fatigue resistance of many alloys has been improved by decreasing the size and number of defects. However, slip band decohesion also causes crack nucleation even when no apparent defect is present. The surface grains must be favorably oriented for slip band decohesion to occur, but not all favorably oriented grains have cracks. Slip along preferred planes plays an important role in crack nucleation. When annealed metals are exposed to cyclic loading, they strain harden. Strain hardening is one of the earliest mechanical responses to fatigue. Initial hardening is rapid and controlled by multiplication of dislocations in the atomic lattice. When the material is first cycled, dislocations glide freely to accommodate large plastic strains. Eventually, the dislocations interact and start to create a substructure of pinned dislocations [29].

The substructure consist of veins for low stain amplitude and cells for higher strain amplitudes [30]. The veins and cell walls consist of high dislocation density while the volume between the veins and cell walls has a much

lower dislocation density. The dislocations can only glide freely in the volume of low density. As the substructure develops, hardening will result because the increased interaction of dislocations constrain their movement. If the cyclic strain amplitude is increased, the cell size decreases which reduces the volume between cells, and hardening continues. Fine slip lines appear on the surface as the dislocation density increases [31].

The rate of hardening gradually decreases until the flow stress becomes constant. The dislocation substructure is saturated and can no longer accommodate strain. Saturation is accompanied by the formation of coarse slip bands which roughen the surface of the grain with extrusions and intrusions. If the surface is polished, small vacancy pits are found in the slip bands. If the specimen is again cycled, the same slip bands roughen the surface. These bands are referred to as persistent slip bands [31].

The persistent slip bands have a distinctive substructure of walls of high dislocation density [32]. The walls are perpendicular to the primary slip direction and stretch across the thickness of the band. The distance between the walls is fairly constant. This substructure is often referred to as a ladder structure [33].

Slip band behavior is not well understood and many different theories exist to explain how the bands accommodate strain [32, 33, 34, 35]. However, it is recognized that the strain is localized in the persistent slip bands and very little strain is accommodated by the volume of material between slip bands. Upon further cycling, cracks form in the persistent slip bands. The cracks are believed to be the combined result of vacancy creation, repulsive dislocation stresses and surface roughening stress concentrations. Experimental evidence show that if the strain amplitude is lower than the saturation point, the strain is accommodated by fine slip associated with pre-saturation dislocation substructure and no cracking takes place [36]. Thus, persistent slip bands are essential to fatigue damage and must be addressed by crack nucleation models.

There are two fundamentally different types of slip-band-induced crack nucleation. One is Forsyth's well known Stage I crack nucleation in which a very small crack (much smaller than the grains size) nucleates along the slip plane very early in life. A crack is evident from crack opening displacement when a static load is applied [1]. The size of the plastic zone is relatively small, being equal to or less than the crack size [37]. The crack propagates in Mode II until it reaches an obstacle, often the grain boundary. This type of crack nucleation has been observed in age hardened aluminum [1] and alloy single crystals [31]. Elastic-plastic crack growth models have been successful in modeling the mean behavior of such alloys down to a very small crack size [38].

The more prevalent though less recognized slip band induced crack nucleation is sudden crack nucleation. In sudden crack nucleation, a slip band which stretches across the grain forms very early in life but no crack is formed. The lack of a crack is evident from no crack opening displacement when a static load is applied [1]. The slip band is not associated with crack beneath the surface [35, 39]. Upon continued cycling, the slip band is blocked by the grain boundary and does not grow in length. However, the depth and the width of the slip band increase slightly until suddenly a crack is form. This slip band crack nucleation behavior is observed in many alloys including steel, aluminum and brass [1, 12, 40]. The crack nucleation model developed in this chapter addresses sudden crack nucleation.

3.2.2 *Micromechanical Crack Nucleation Models*

Models used to predict scatter in crack nucleation response must have two attributes. They must be quantitative with regards to the number of cycles needed to produce a crack to a specific size if they are to be used for life-time predictions. The models must also be able to address the microstructural parameters in order to provide a physical link between the microstructure and the fatigue behavior. Although the literature contains numerous expressions for modeling the propagation rate of fatigue cracks as discussed later, only a limited number of analytical crack nucleation models exist. Most all of these models use dislocation theory [41] to model fatigue damage accumulation as the build up of a continuous array of dislocations [42].

Microstructural models which predict crack nucleation life and crack nucleation size have been proposed independently by Tanaka and Mura [34] and Chang *et al.* [43]. Both of these models predict damage accumulation through irreversible dislocation pile-up at microstructural obstacles. Cracks nucleate when a critical strain energy is exceeded.

Models are available to address a wide variety of crack nucleation mechanism including:

- slip band cracking within a grain [34]
- grain boundary cracking [34]
- matrix/inclusion interface cracking [34]
- cracks emanating from inclusions [34,43]
- cracks emanating from notches [44]

The models have been modified to account for partial reversibility and random load amplitudes[45]. The crack

nucleation models had to be modified by the authors to include the effects of additional random variables.

The models are consistent with the Coffin-Manson relationship for fatigue crack initiation [34, 46], the Petch equation for the grain size dependency of the fatigue strength [34] and the Palmgren-Miner law of damage accumulation for variable amplitude loads.

The crack nucleation model used in this study is based on one proposed by Tanaka and Mura [34] in which the forward and reverse plastic flow within the persistent slip band of a surface grain is related to the creation of dislocations of opposite signs on closely spaced planes. This model is applicable to metallic components for which crack nucleation takes place by transgranular shear stress fracture and is outlined below.

As a load greater than the local yield stress is applied to grain with diameter *d*, dislocations are generated and move along the slip plane as shown in Figure 2. The dislocations pile up at the grain boundary which acts as an obstacle to dislocation movement. The dislocation movement is assumed to be irreversible such that when the reverse load is applied, dislocations of the opposite sign pile up on a closely spaced plane. Since the residual load from the back stress of the positive dislocations act in the same direction as the reverse applied load, unloading will cause negative dislocation movement. During each of the subsequent load cycles, the number of dislocations monotonically increase.

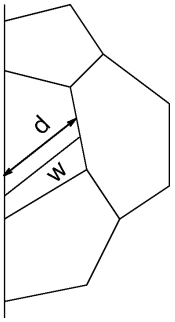

Figure 2: Slip band of width *w* interacting developing on grain of size *d*.

On the first loading, the equilibrium condition can be expressed as

$$\tau_1^D + (\tau_1 - k) = 0 \tag{1}$$

where k is the frictional stress which must be overcome to move dislocations, τ_1 is the applied shear stress (τ_1 must be greater than k for damage to accumulation to occur), and τ_1^D is the back stress caused by the dislocations. If the dislocation density $D_1(x)$ along the slip plane is assumed to be continuous [42]

$$\tau_1^D = A\int_{-r}^{r} \frac{D_1(x')}{x - x'}dx'$$

$A = G/2\pi(1-\upsilon)$ for edge dislocations

$A = G/2\pi$ for screw dislocations

where r is the grain radius, G is the shear modulus and ν is Poisson's ratio. Substituting Eq. (2) into Eq. (1) creates a singular integral equation which is solved for $D_1(x)$ using the inversion formula of Muskhelishvili [47] for unbounded dislocation density at the grain boundary

$$D_1(x) = \frac{(\tau_1 - k)x}{\pi A\sqrt{r^2 - x^2}} \tag{3}$$

The incremental increase of dislocation density $\Delta D(x)$ with each load cycle is

$$D_1(x) = \frac{(\Delta\tau_1 - 2k)x}{\pi A\sqrt{r^2 - x^2}} \tag{4}$$

The slip displacement $\phi(x)$ due to the increment $\Delta D(x)$ is

$$\phi(x) = \int_{x}^{r} \Delta D(x)\,dx \tag{5}$$

The plastic strain increment $\Delta\gamma$ is

$$\Delta\gamma = \int_{-r}^{r} \phi(x)\,dx = \frac{(\Delta\tau - 2k)r^2}{2A} \tag{6}$$

such that the constitutive equation is

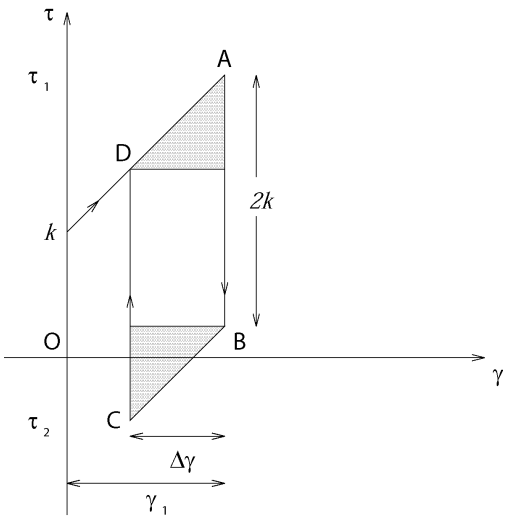

Figure 3: Stress-strain hysteresis loop.

$$\gamma = \frac{(\tau - 2k) r^2}{2A} \tag{7}$$

which describes the stress-strain hysteresis loop in Figure 3.

During the first forward loading of stress τ_1, the material hardens for any stress above *k*. On reverse loading to τ_2, the path ABC is followed. On subsequent forward loading, the path CDA is followed. The amount of plastic strain increment is a linear function of $(\tau - k)$. The dislocation strain energy is the same for forward and reverse loading except the first loading. The incremental stored dislocation strain energy ΔU corresponds to the shaded area of Figure 3.

$$\Delta U = \Delta\gamma(\Delta\tau - 2k) \tag{8}$$

The energy associated with the unshaded area of Figure 3 is the dissipated work against the frictional stress *k*. Crack nucleation takes place when the total stored energy after N_n cycles is equal to the fracture energy of the grain.

$$N_n \Delta U = 2rW_s \tag{9}$$

$$N_n = \frac{4GW_s}{(\Delta\tau - 2k)^2 \pi(1-\nu)d} \tag{10}$$

where *d* is the grain diameter and W_s is the specific fracture energy per unit area.

The probabilistic mesomechanical fatigue model calculates the crack nucleation life using Eq. (10) in a slightly modified form. The modification is that $\Delta\tau$ is replaced with $\Delta\sigma / M$ where $\Delta\sigma$ is the applied axial stress and *M* is the grain orientation factor.

The model has several assumptions and limitations.

1. *The grain is homogeneous*. The dislocations are free to move to the grain boundaries i.e., no subgrain structure exists to pin or disrupt dislocation movement. Although the grain is homogeneous it is not isotropic.
2. *Damage accumulates on a single planar slip system*. In general, grains within a polycrystalline aggregate are not free to deform but are constrained by neighboring grains. Crack nucleation takes place on the surface grains which are not as constrained as grains embedded in the interior. Surface grain are able to accommodate more strain on the primary slip system [48]. The model can only be directly used on alloys that show planar slip.
3. *The crack nucleation size is equal to the grain size*. Although loading has been shown to effect the nucleation size (the crack size at Mode II to Mode I transition) [3, 4], experimental evidence suggest that the nucleation size is on the order of the grain size [5, 6, 7].
4. *The dislocation movement is irreversible and dipoles pile-up monotonically at the grain boundaries*. It is reasonable to expect some of the dislocations to move back into the interior of the grain upon reverse loading or be annihilated by back stresses. Theoretical investigations on how to account for the partial reversibility of slip band formation have been inconclusive [45, 49, 50]. However, there is experimental evidence that this reverse movement is small [34].
5. *The number of cycles to saturation are negligible*. This assumption is reasonable for many materials under certain loading conditions [7, 31].

Equation (10) is necessarily a simplification of the complex phenomenon of slip band cracking. It does not directly address the effect of vacancy creation or the stress concentration of the surface roughening. However, the model is attractive because the fatigue life is inversely proportional to the square of the plastic strain amplitude which is in agreement with the Coffin-Manson empirical equation for fatigue. Equation (10) can be rewritten as

$$\Delta\tau = 2k + \left(\frac{4GW_s}{\pi N_n (1-\nu)}\right)^{\frac{1}{2}} d^{-\frac{1}{2}} \tag{11}$$

which is in the form of the Hall-Petch equation for the dependence of fatigue strength on grain size.

3.3 Microstructurally Small Crack Growth

3.3.1 *Micromechanics of Small Crack Growth*

The experimentally observable parameter that has been correlated to the varying small crack growth rate is the crack opening displacement (COD) [37]

$$\frac{da}{dN} = C'(\Delta COD)^{n'} \tag{12}$$

where a is the crack length, N is the number of cycles, C' and n' are empirical constants based on material testing. The COD is measure of the amount of damage associated with the crack tip. The larger the COD the higher the crack growth rate. This phenomenon was first observed by Laird and Smith [51] and has been well established in long crack growth [52, 53]. The exponent n' has been found to have a value near unity when the COD is replaced by crack tip opening displacement (CTOD)

$$\frac{da}{dN} = C'\Delta\phi_t \tag{13}$$

where the CTOD, denoted by ϕ_t is measured at the location of crack extension for the previous cycle. The direct proportionality of Eq (13) has been observed in small crack growth of aluminum, nickel and titanium alloys [54]. Equation (13) has also been shown to correlate the behavior between small and long crack growth [55]. Nisitani and Takao [1] showed that small crack arrest could be associated with no CTOD. Tanaka *et al*. [56] showed that regressing data to Eq (13) showed much less scatter than exponential models based on ΔK or ΔJ. Also, developing models for three different materials; copper, mild steel and stainless steel, produced very similar values for C' and n'. (The exponent n' was not unity because the COD measurements were made on the specimen surface at the center of the crack.) It appears as though the relationship between da/dN and $\Delta\phi_t$ is more of an intrinsic material behavior than models based on ΔK or ΔJ.

Determining C' for small crack growth has been performed through direct microscopic observations [1]. However, there has been limited success in using ΔK or ΔJ data to determine C'.

CTOD can be shown to be related to the J integral through

$$\phi_t = \alpha\frac{J}{\sigma_0} \tag{14}$$

where σ_0 is the bulk yield strength and α is nearly unity [57]. Assuming elastic perfectly plastic behavior, CTOD can be related to K through

$$\phi_t = \frac{2K^2}{\pi\sigma_0\upsilon} \tag{15}$$

where ν is Poisson's ratio. Combining Eqs. (13) and (15)

$$\frac{da}{dN} = \frac{C'\Delta K^2}{2\pi\sigma_0\upsilon} \tag{16}$$

which is the form of a second-order Paris equation. Determining C' using da/dN vs. ΔK data is straight forward for alloys that are governed by a second-order Paris relationship. Donahue *et al*. [58] have compiled an extensive list of data that fit a second-order Paris equation. They find a C' value of about 0.1 fits most of the data. However, in general the Paris exponent is not expected to be 2.

It is interesting to note that McEvely [59] presents data form several sources which shows that a well defined region of constant slope is seldom found in the Paris fit. The slope was found to vary with ΔK and have a value of 2 at low ΔK (the region of interest in the present study) and increase at higher ΔK. Also, there has been some success [60] with correlating data to

$$\frac{da}{dN} = C''\Delta K_{eff}^2 \tag{17}$$

where ΔK_{eff} is the effective ΔK which is the applied ΔK minus the ΔK when the crack first opens. However, the measurement of ΔK_{eff} still requires direct observations at the crack tip. The relationship in Eq.(13) is assumed to be valid and will be used in the present study.

3.3.2 *Small Crack Growth Models*

Two basic approaches have been used to model small crack growth behavior: modify a continuum mechanics based stress intensity factor, *K*, to account for the microstructural heterogeneity or, explicitly model the damage ahead of the crack tip using dislocation theory. Hobson [61] presented a simple continuum based model in which the crack growth rate is related to the distance between the crack tip and the nearest grain boundary. All of the model parameters are determined by fitting the model to experimental data. Chan and Lankford [37] modifies *K* to account for grain size and orientation using a simple analytical approach. Chan and Lankford [62] uses a more rigorous analytical approach to modify *K* for microstructural effects and large scale yielding. They introduce the concept of microstructural dissimilitude which accounts for the fact that small cracks actually lie in relatively few grains. Similitude can be assumed when the crack front interrogates enough grains such that the material properties averaged along the crack front have the same value as the bulk material properties. When the crack front interrogates relatively few grains, the average material properties at the crack front can vary significantly from the bulk properties, hence, microstructural dissimilitude. The number of grains interrogated by the crack front necessary to assume similitude depends on the amount of scatter in the local material properties. Also, by using an equivalent properties model that effectively averages the microstructural environment interrogated by the two dimensional crack front, Chan and Lankford [37] were able to reduce small crack growth to a one dimensional problem.

Gerberich and Moody [63] used a modified continuum approach to address the semi-cohesive zone associated with selective cleavage in the microstructure at the crack tip for Ti-6Al-4V. Using this model, they were able to predict the mean grain size effect on threshold for titanium alloys.

Bilby and Eshelby [42] described the damage ahead of the crack tip using the theory of continuous dislocations. The models are equivalent to the Dugdale [64] model found by a different method. Weertman [65] used the model of Bilby *et al.* [66] to develop a fatigue crack growth law and later used dislocation theory to developed a *K* for short cracks [67].

Several researches have extended Bilby's model to account for microstructural effects. Taira *et al.* [68] obtained a model for a crack tip slip band blocked by a grain boundary. Tanaka *et al.* [69] extended Taira's model to slip band propagation through grain boundaries. The CTOD predicted by the model was found to be equivalent to that predicted by both Morris *et al.* [70] and de los Rios *et al.* [71]. Navarro *et al.* [72] used an equivalent model to Tanaka's to describe small and short crack growth. The models predicted the bounds on the variation in small crack growth.

Many statistical and probabilistic crack growth models can be found in the literature. The Markov based models [73] describe the crack growth rate scatter as a process in which the amount of crack extension for each cycle is a random function. The Paris-based models describe the crack growth rate scatter by allowing the material property parameters to be random [74]. A common feature of these models is that the random nature of the crack growth is not related to microstructural variables. Thus, these models are not useful in understanding small crack growth behavior.

Limited work has been reported on models which directly addresses the statistical aspects of small crack growth. Morris *et al.* [75] used Monte Carlo simulation to model the crack initiation behavior of aluminum smooth round bars. They used the crack nucleation model of Chang *et al.* [43] and a modified, continuum-based-*K*, small crack growth model. The random variables included crystallographic orientation, grain diameter, inclusion diameter, and an experimentally determined material parameter associated with the fracture strength of the inclusion. The statistical distributions of the random variables were not discussed. The predicted results compared favorably to the experimental observations. Tanaka *et al.* [56] used Monte Carlo simulation to predict the general behavior of small crack growth. They used the small crack growth model of Tanaka *et al.* [69]. The random variables included grain size, grain frictional stress, and an independent grain boundary strength. A two-parameter Weibull distribution was assumed for all of the random variables. They extended the model to include two-phase materials. Trends predicted by the model compared favorably with general trends observed in small crack growth behavior.

3.3.3 *A Model Based on Continuously Distributed Dislocations*

The model developed in the present study follows the approach used by Tanaka *et al.* [69]. The approach is outlined below for Mode II (sliding) crack growth. The solution for Mode I (tensile) crack growth is obtained through the simple transformations discussed at the end of the section.

Assume a crack has length *a* and the crack tip lies within a grain as shown in Figure 4. As load is applied, dislocations are emitted from the crack tip creating a slip band with dislocation density ($D(x)>0$) as represented by the length *w* in Figure 4. For low stress (where the applied stress is less than the stress needed to move dislocations) and the slip band tip far from the gain boundary ($c<d$). A condition called the *equilibrium slip band* exist.

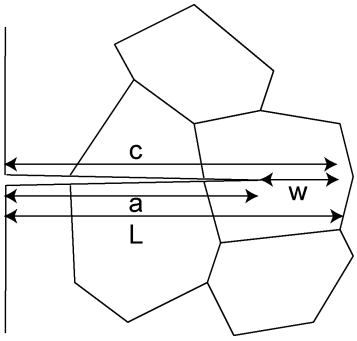

Figure 4: Crack tip in a grain.

The solution for the equilibrium slip band was obtained by Bilby *et al*. [66]. The equilibrium condition can be expressed as

$$\tau^D + \tau^0 = 0$$
$$\tau^D = A\int_{-c}^{c} \frac{D(x')}{x - x'}dx'$$
$$A = \begin{cases} G/2\pi(1-\upsilon) & \text{for edge dislocations} \\ G/2\pi & \text{for screw dislocations} \end{cases} \quad (18)$$
$$\tau^0 = \begin{cases} \tau & x < a \\ \tau - k_1 & a < x < c \end{cases}$$

where τ is the resolved applied shear stress, τ^D is the back stress caused by the dislocations, G is the shear modulus, and k_1 is the friction stress (which must be overcome to move dislocations) of the grain in which the crack tip and slip band lie. The size of the slip band w is determined from the condition of vanishing dislocation density at the slip band tip.

$$w = c - a \quad (19)$$

$$\frac{a}{c} = \cos\left(\frac{\pi\tau}{2k_1}\right) \quad (20)$$

The dislocation density $D(x)$ is obtained by solving the singular integral Eq. (18) using the inversion formula of Muskhelishvili [47] for unbounded dislocation density at the crack tip.

$$D(x) = \frac{k_1}{\pi^2 A} f(x;c,a)$$
$$f(x;c,a) = \ln\left|\frac{x\sqrt{c^2-a^2} + a\sqrt{c^2-x^2}}{x\sqrt{c^2-a^2} - a\sqrt{c^2-x^2}}\right| \quad (21)$$

The crack tip sliding displacement (CTSD) is

$$\phi_t = \frac{2k_1 a}{\pi^2 A}\ln\frac{c}{a}$$
$$= \frac{2k_1 a}{\pi^2 A}\ln\left[\sec\left(\frac{\pi\tau}{2k_1}\right)\right] \quad (22)$$

As the crack grows, the tip of the slip band will eventually be blocked at the grain boundary. This condition is called the *blocked slip band*.

The solution for the blocked slip band was obtained by Taira *et al*. [68]. The size of the slip band is simply

$$w = c - a$$
$$c = L \quad (23)$$

The dislocation density $D(x)$ is obtained by solving the singular integral Eq. (18) using the inversion formula of Muskhelishvili [47] for unbounded dislocation density at the crack tip and the slip band tip.

$$D(x) = \frac{\beta\tau}{\pi A}\frac{x}{\sqrt{c^2-x^2}} + \frac{k_1}{\pi^2 A} f(x;c,a)$$
$$\beta = 1 - \frac{2k_1}{\pi\tau}\arccos\frac{a}{c} \quad (24)$$

The microscopic stress intensity factor K_m at the tip of the slip band is similar to the crack tip stress intensity factor and is defined as

$$K_m = \pi A\sqrt{2\pi}\lim_{x\to c}\left[\sqrt{c-x}D(x)\right]$$
$$= \beta\tau\sqrt{\pi c} \quad (25)$$

The CTSD is

$$\phi_t = \frac{\beta\tau}{\pi A}\sqrt{c^2-x^2} + \frac{2k_1 a}{\pi^2 A}\ln\frac{c}{a} \quad (26)$$

As the crack grows, K_m increases. For the crack to overcome the grain boundary obstacle and propagate into the subsequent grain, K_m must exceed the critical microscopic stress intensity factor K_{mc} provided by the grain boundary. If as $a \to c$, K_m does not exceed K_{mc}, then the $\text{CTSD} \to 0$ and the crack growth arrest. If K_m exceeds K_{mc}, the slip band tip propagates into the next grain and a condition called the *propagating slip band* exist.

The solution for the propagated slip band was obtained by Tanaka *et al*. [69]. The equilibrium condition is the same as Eq.(18) except

$$\tau^0 = \begin{cases} \tau & x < a \\ \tau - k_1 & a < x < L \\ \tau - k_2 & L < x < c \end{cases}$$

where k_2 is the frictional stress in the second grain. The size of the slip band zone is determined from the condition of vanishing dislocation density at the slip band tip.

$$\arccos\frac{a}{c} + \left(\frac{k_2}{k_1} - 1\right)\arccos\frac{L}{c} = \frac{\pi\tau}{2k_1} \tag{27}$$

The dislocation density and CTSD are determined in a similar manner as before.

$$\begin{aligned} D(x) &= \frac{k_1}{\pi^2 A} f(x;c,a) + \frac{(k_2 - k_1)}{\pi^2 A} f(x;c,L) \\ \phi_t &= \frac{2k_1 a}{\pi^2 A}\ln\frac{c}{a} + \frac{(k_2 - k_1)}{\pi^2 A} g(a;c,L) \\ g(a;c,L) &= L\ln\left|\frac{\sqrt{c^2 - L^2} + \sqrt{c^2 - a^2}}{\sqrt{c^2 - L^2} - \sqrt{c^2 - a^2}}\right| \\ &\quad - a\ln\left|\frac{a\sqrt{c^2 - L^2} + L\sqrt{c^2 - a^2}}{a\sqrt{c^2 - L^2} - L\sqrt{c^2 - a^2}}\right| \end{aligned} \tag{28}$$

Tanaka *et al*. [56] solve for the case in which the slip band extends over several grains as shown in Figure 5. If the crack tip is in the j^{th} grain and the slip band is in the n^{th} grain, the equilibrium condition is the same as Eq.(18) except

$$\tau^0 = \begin{cases} \tau & x < a \\ \tau - k_1 & a < x < L_j \\ \vdots & \vdots \\ \tau - k_2 & L_{n-1} < x < c \end{cases}$$

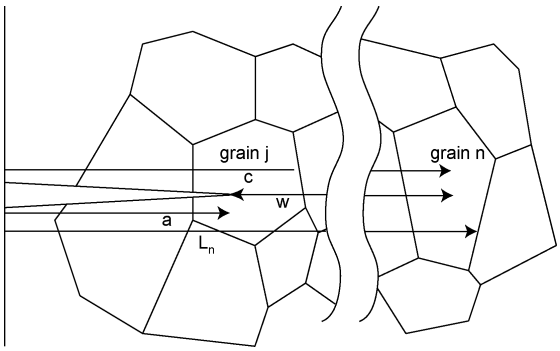

Figure 5: Crack tip slip band in multiple grains.

The size of the slip band zone can be found from

$$\begin{aligned} 0 &= \frac{\pi\tau}{2} - k_j \arccos\frac{a}{c} \\ &\quad - \sum_{i=j+1}^{n} (k_i - k_{i-1})\arccos\left(\frac{L_{i-1}}{c}\right) \end{aligned} \tag{29}$$

The CTSD is given by

$$\phi_t = \frac{2k_j a}{\pi^2 A}\ln\frac{c}{a} + \sum_{i=j+1}^{n}\frac{(k_i - k_{i-1})}{\pi^2 A} g(a;c,L_{i-1}) \tag{30}$$

For the crack tip in the j^{th} grain and the slip band blocked in the n^{th} grain, the size of the slip band zone is

$$w = L_n - a \tag{31}$$

The CTSD is given by

$$\begin{aligned}\phi_t &= \frac{\beta\tau}{\pi A}\sqrt{c^2-a^2}+\frac{2k_j a}{\pi^2 A}\ln\frac{c}{a}\\ &\quad+\sum_{i=j+1}^{n}\frac{(k_i-k_{i-1})}{\pi^2 A}g(a;c,L_{i-1})\\ \beta &= 1-\frac{2k_1}{\pi\tau}\arccos\frac{a}{c}\\ &\quad-\sum_{i=j+1}^{n}\frac{2(k_i-k_{i-1})}{\pi\tau}\arccos\left(\frac{L_{i-1}}{c}\right)\end{aligned} \tag{32}$$

The microscopic stress intensity factor is

$$K_m = \beta\tau\sqrt{\pi c} \tag{33}$$

The above model allows for grain to grain variation in grain size and frictional stress.

In the present study, the Tanaka *et al.* [69] model is extended to include the variation in the microstress and the grain orientation by allowing grain to grain variation in the applied resolved shear stress τ.

Consider a crack with the crack tip in the j^{th} grain and the slip band tip in the n^{th} grain. The equilibrium condition is the same as Eq.(18) except

$$\tau^0 = \begin{cases}\tau_j & x<a\\ \tau_j-k_j & a<x<L_j\\ \vdots & \vdots\\ \tau_n-k_n & L_{n-1}<x<c\end{cases}$$

For the propagated slip band, the size of the slip band zone can be found from

$$\begin{aligned}0 &= \frac{\pi\tau_j}{2}-k_j\arccos\frac{a}{c}\\ &\quad-\sum_{i=j+1}^{n}\left((\tau_{i-1}-k_{i-1})-(\tau_i-k_i)\right)\arccos\left(\frac{L_{i-1}}{c}\right)\end{aligned} \tag{34}$$

The CTSD is given by

$$\begin{aligned}\phi_t &= +\frac{2k_j a}{\pi^2 A}\ln\frac{c}{a}\\ &\quad+\sum_{i=j+1}^{n}\frac{(\tau_{i-1}-k_{i-1})-(\tau_i-k_i)}{\pi^2 A}g(a;c,L_{i-1})\end{aligned} \tag{35}$$

For the blocked slip band, the size of the slip band zone is

$$w = L_n - a \tag{36}$$

The CTSD is given by

$$\begin{aligned}\phi_t &= \frac{\beta\tau}{\pi A}\sqrt{c^2-a^2}+\frac{2k_j a}{\pi^2 A}\ln\frac{c}{a}\\ &\quad+\sum_{i=j+1}^{n}\frac{(\tau_{i-1}-k_{i-1})-(\tau_i-k_i)}{\pi^2 A}g(a;c,L_{i-1})\\ \beta &= 1-\frac{2k_1}{\pi\tau_j}\arccos\frac{a}{c}\\ &\quad-\sum_{i=j+1}^{n}\frac{2\left((\tau_{i-1}-k_{i-1})-(\tau_i-k_i)\right)}{\pi\tau_j}\arccos\left(\frac{L_{i-1}}{c}\right)\end{aligned} \tag{37}$$

The microscopic stress intensity factor is

$$K_m = \beta\tau\sqrt{\pi c} \tag{38}$$

The solution for mode I loading is easily obtained through the following substitutions:

$$\tau \rightarrow c$$

$$\text{CTSD} \rightarrow \text{CTOD}$$

3.4 Long Crack Growth

The linear elastic crack growth is modeled using the Paris law representation of a surface crack in a semi infinite body subjected to a constant stress cycle.

$$\frac{da}{dN} = C\Delta K^n$$
$$\Delta K = \beta \Delta s_{xx} \sqrt{a} \tag{39}$$

where a is the crack length, N is cycles, ΔK is the stress intensity factor, Δs_{xx} is the stress range, β is the geometry constant $\left(1.12\sqrt{\pi}\right)$, and C and n are material properties.

Expanding ΔK and integrating both sides

$$C\left(\beta \Delta s_{xx}\right)^n \int_0^{N_g} dN = \int_{a_i}^{a_f} a^{-\frac{n}{2}} da \tag{40}$$

$$N_g = \frac{a_i^{1-\frac{n}{2}} - a_f^{1-\frac{n}{2}}}{C\Delta s_{xx}^n \beta^n \left(\frac{n}{2}-1\right)}; n \neq 2 \tag{41}$$

where, N_g is the number of cycles needed for the crack to grow to failure, a_i is the initial crack size and a_f is the failure crack size.

If $n > 2$ and $a_i \ll a_f$, then $a_i^{1-\frac{n}{2}} \gg a_f^{1-\frac{n}{2}}$ and Eq. (41) can be written as

$$N_g = \frac{a_i^{1-\frac{n}{2}}}{C\Delta s_{xx}^n \beta^n \left(\frac{n}{2}-1\right)}; n \neq 2 \tag{42}$$

4 Estimate of Random Variable Statistics

The variables in the damage accumulation models that are considered random in the probabilistic microstructural fatigue algorithm are:

- Grain Size
- Surface Grain Orientation
- Interior Grain Orientation
- Frictional Shear Stress
- Paris Law Coefficient

The mean values of the random variables such as grain size and frictional strength can vary significantly with heat treatment and other processes. The mean values can often be easily determined from the information traditionally reported in the literature. However, information needed to determine the statistical variation and the distributions types of the random variables is usually not reported. Nor is this information gathered during routine material characterizations performed by the aerospace industries. Luckily, specific studies to gather the needed information have been performed. These studies are used to estimate the random variables for the Phase I effort and are discussed below.

4.1 Grain Size

Empirical observations have indicated that the scatter in grain size for *natural grain growth* i.e., cast polycrystalline structures, is insensitive to material. This has been observed in pure metals, complex alloys, and inorganic ceramics [76]. This phenomenon has been attributed to the well behaved kinetics that determines natural

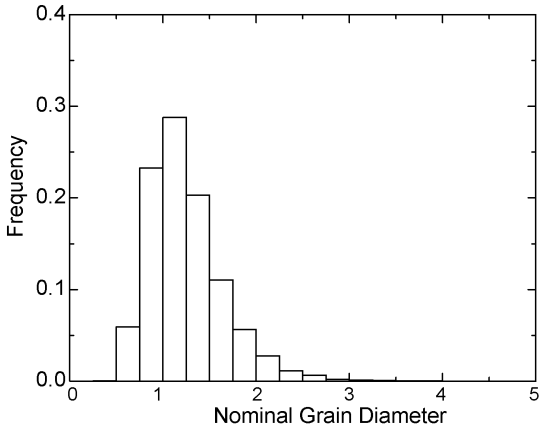

Figure 6: Grain diameter distribution.

grain growth.

Kurtz and Carpay [77] performed extensive grain volume measurements on Ni-Zn ferrites by way of planar sectioning, and describe the grain size by the equivalent spherical volume diameter. They determined the grain size distribution for 7 different mean grain size microstructures measuring several thousand grains for each microstructure. They found the COV to vary between 0.3 and 0.4. The COV was independent of mean grain size. The distribution was accurately described by a lognormal distribution with the maximum to mean grain size ratio of about 2.7.

Kumar *et al.* [78] investigated the grain size distribution using Monte Carlo techniques and a Voronoi tessellation technique, which closely model the grain topography of polycrystals. They found a COV of about 0.4. The lognormal distribution was a good fit up to about 5000 grains. Simulating greater than 100,000 grains, they found the gamma distribution to be a best fit. The gamma distribution may well be an artifact of the modeling technique and not intrinsic to the grain size distribution. Voronoi tessellation uses the Poisson process to generate the grain geometry and the gamma distribution is directly related to the Poisson process [79]. In the present study, a lognormal distribution with a COV of 0.4 as shown in Figure 6 will be assumed.

The bulk of the grains measured in the above research were interior grains. A distinction must be made between the size of the surface grains and those in the interior. Although the surface grains may account for only a small fraction of the total grains within a component, understanding the properties of the surface grains is paramount because they play an important role in crack nucleation and small crack growth.

The surface effectively slices each grain in a random manner such that

$$l = d_s \cos\theta \tag{43}$$

where l is the surface length, d_s is the grain diameter, and θ is the random angle of incidence as shown in Figure 7. For an arbitrary cut through the grain, θ is uniformly distributed between 0 and $\pi/2$. The distribution of d_s can be determined from

$$l = d_s \cos\left(\frac{\pi}{2}u\right) \tag{44}$$

where d_s is lognormally distributed as shown in Figure 6 and u is the standard uniform random variable.

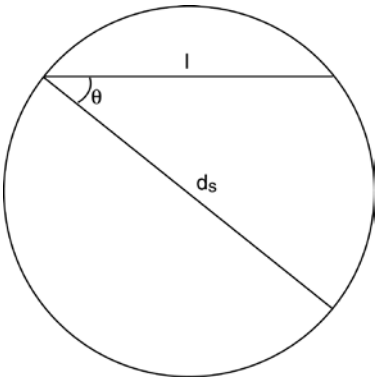

Figure 7: Line cutting across the grain.

Monte Carlo simulation was used to evaluate the distribution of d_s as shown in Figure 8. Comparing Figure 8 to Figure 6 shows that the average diameter of the surface grains is smaller than the interior grains. The increase width of the surface grain distribution indicates that the scatter in the surface grains diameter is larger than the interior grains.

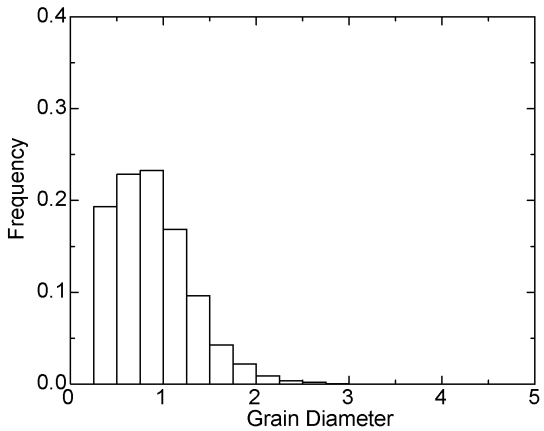

Figure 8: Surface grain size distribution.

4.2 Grain Orientation

In metallic structures, slip can occur on many planes in several directions. All orientations for cubic structures can be defined within the standard stereographic triangle [80].

The orientation dependence of the reciprocal Schmid factor is shown in Figure 9. Figure 9 represents axially loaded grains that are free to deform such that slip occurs on a single plane.

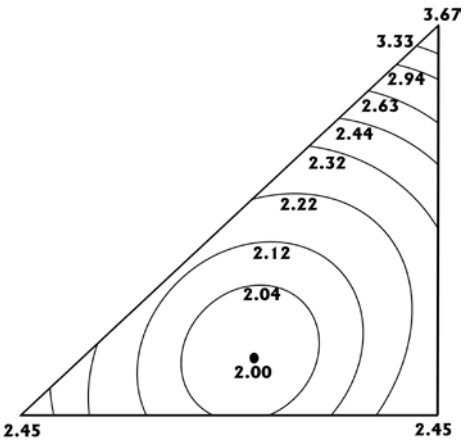

Figure 9: Orientation dependence of reciprocal Schmid factor.

However, grains within a polycrystalline aggregate are not free to deform but are constrained by neighboring grains.

Taylor [81] determined the equivalent to the reciprocal Schmid factor, *M*, for axisymmetric flow in a face-centered cubic polycrystal. He assumed the frictional stress was the same for each slip system. He also assumed that each grain is acted upon by the same applied strain as the macroscopic strain. Taylor assumed the active slip systems are those for which the sum of the shear strains is a minimum. Bishop and Hill [82] later showed that the Taylor analysis is equivalent to a maximum work principle. This quantity is referred to as the Taylor factor. Chin and Mammel [83] developed a computer model based on the Taylor analysis and found the Taylor factor for slip on other orientations in cubic polycrystals.

Crack nucleation takes place on the surface grains. It is difficult to determine *M* for the surface grains which are not as constrained as grains embedded in the interior. Surface grains are able to accommodate more strain on the primary slip system. Although slip band formation and crack nucleation on secondary planes is not uncommon, experimental evidence shows that cracks tend to nucleate on the primary slip plane [84]. In reality, the deformation of surface grains is somewhere between free deformation and fully constrained. The reciprocal Schmid factor is used to describe the surface grains and the Taylor factor is used to describe the interior grains in the present study.

The orientations of the grains of an untextured polycrystalline material can be expressed as a uniform distribution of points within the stereographic triangle. To determine the statistical distribution of the Schmid factor for the randomly oriented grains, response surface was generated to approximate the Schmid factor within the stereographic triangles of Figure 10. A Monte Carlo simulation was used to generated points uniformly throughout the stereographic triangle as shown in Figure 10. (A similar technique has since been published by Ono *et al*. [85]). The response surface used to determine the Schmid factor for each of these points and the scatter among the Schmid factor is determined. The probability density function (PDF) of *M* is shown in Figure 11. The mean value of the distribution is 2.21 which is in agreement with other analytical findings [86]. The predicted PMF of *M* compares favorably to the experimentally determined value for 203 surface grains of an untextured pure iron [87] as shown in Figure 11.

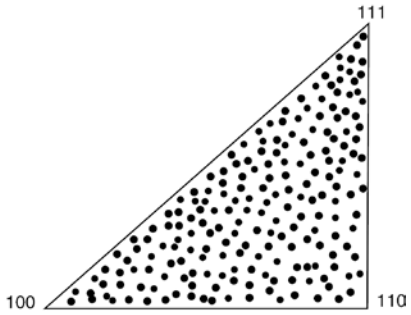

Figure 10: Uniform distribution of points throughout the stereographic triangle.

Using the same Monte Carlo technique, the PDF of the Taylor factor for an untextured polycrystal are shown in Figure 12. The mean value of the distribution is 3.07 which is in agreement with analytical and experimental findings [88]. The predicted PDF of *M* determined in the present study compares favorably to the analytical results of Sun *et al*. [89]. They determined the PDF of the Taylor factor using the computer solution of Chin and Mammel [83] and considering all possible crystallographic orientations.

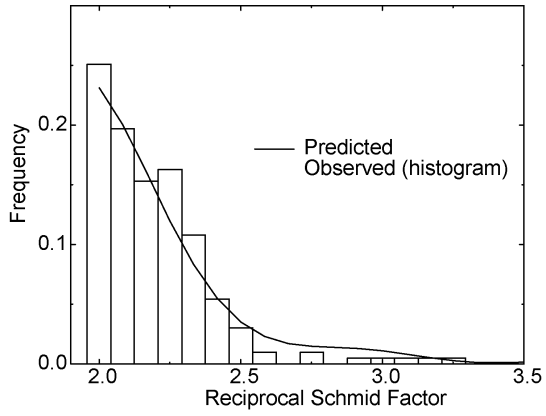

Figure 11: Probability density function of the reciprocal Schmid factor.

4.3 Frictional Shear Stress

The frictional stress is the stress that must be overcome for dislocations to move within a grain. The frictional stress can be thought of as the local yield stress. Because of the crystallographic orientation of the grain, yielding takes place on well defined planes (in the low Γ planar slip alloys). Experimental observations have shown that the frictional stress is nearly uniform across the grain [90].

There is little direct data available in the literature on the statistical distribution of the frictional stress. A rigorous

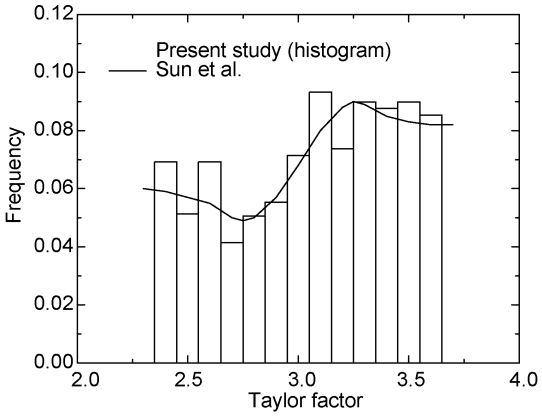

Figure 12: Probability density function of the Taylor factor.

numerical determination of the grain-to-grain scatter in frictional stress has not been made. However, empirical observations provide some insight into the behavior of the scatter.

Taira *et al*. [3] experimentally observed the minimum cyclic stress for which slip bands formed in three different mean grain size microstructures of low-carbon steel. The applied stress was below the fatigue limit and slip bands formed in very few grains. They found that the minimum frictional stress is independent of mean grain size. The minimum frictional stress was nearly equal to the frictional stress predicted by the Petch relationship for the fatigue limit, expressed as

$$\sigma_{fl} = k_{fl} + \frac{K_m}{\sqrt{d}} \tag{45}$$

where σ_{fl} is the fatigue limit, k_{fl} is the frictional stress of the grains participating in fatigue and K_m is the microscopic stress intensity factor.

Taira *et al*. [3] used the Petch relationship for flow stress to determine the frictional stress for applied loads up to 5 % plastic strain. As the load increased, more and more grains produced slip bands. An indication of the scatter can be made by comparing the frictional stress determined at high applied load to the frictional stress at low applied load. At high applied load, many grains produce slip bands and this frictional stress may be thought of as the frictional stress of the nominal grain. At low applied load, only a few grains produce slip bands and this frictional stress may be thought of as the frictional stress of the weakest grain.

This method is not rigorous because the variation in the microstress is not taken into account. In addition, it is difficult to determine the shape of the distribution. In the present study a two parameter Weibull distribution is assumed and fitted to the data in Taira *et al*. [3]. The parameters of the Weibull distribution are determined by taking the frictional stress determined from the 5% plastic strain test, $k_{0.5} = 340MPa$,to be the frictional stress of the 50 percentile grain and the frictional stress from the fatigue limit test , $k_{fl} = 110MPa$, is taken to be the frictional stress of the 1 percentile grain. This gives a normalized Weibull distribution with a shape factor $\beta_k = 3.7$ and a characteristic value $\eta_k = 1.12$ that yields a mean value of 1 and a COV of 0.3. Tanaka *et al*. [56] indicate that a two parameter Weibull distribution with COV between 0.3 and 0.7 can be used to describe the frictional stress.

4.3.1 *Applied Micro-Stress*

Because each grain acts as an anisotropic single crystal, the actual loading on an individual grain is caused by the deformation of the surrounding grains, which are in turn loaded by the deformations of each of their surrounding grains. Therefore, the micro-stress distribution is a function of the anisotropic deformation of all on the grains that compose the structure.

Barenblatt [91] proposed a theoretical model to describe the micro-stress field. Many simplifying assumptions were necessary to make the model tractable. Zhao and Tryon [92] investigated the micro-stress field for a single phase nickel alloy using finite elements and Voronoi tessellation to produce a model that closely approximates the microstructure. They modeled a statistical volume element with 200 grains. Each grain was modeled as an anisotropic single crystal with several hundred finite elements per grain. An elastic analysis was performed in which a uniaxial macroscopic load was applied. The von Mises stress at the grain interiors could be described by a normal distribution with a mean equal to the applied macroscopic stress and a COV of 0.25. The stress distribution of the surface grains was found to be the same as the interior grains. The COV was a function of the elastic anisotropy of the material.

In this paper the micro-stress will be assumed to have a normal distribution with a mean value equal to the applied load s_{xx} and a COV of 0.25.

5 Monte Carlo Simulation of Each Stage of Damage Accumulation

The Monte Carlo simulation of the fatigue damage accumulation is used to determine the probability that a

component will fail at a given number of cycles. The component to be modeled is a smooth round bar subjected to constant cyclic load amplitude. The global loading is assumed to be uniform throughout the gage section. A single RVE is also assumed to be valid throughout the gage section. The material is assumed to be a single phase polycrystal such as a nickel superalloy or high strength steel. This analysis simulates an empirical fatigue characterization test in which specimens are cycled to failure and the number of cycles at failure is recorded. The Monte Carlo simulation produced the same data. A bar is chosen (simulated) and cycled to failure. The number of cycles at failure are recorded.

The basic low of the simulation is as follows

1. A bar is chosen and the grains of the bar are generated using the statistical distributions described above. Each grain has a distinct size, orientation, frictional strength and microstress.
2. A crack is nucleated in a surface grain and the cycles to failure are found using the model described earlier.
3. Each crack then grows through the microstructure via the small and then long crack growth models described earlier.
4. Another grain is chosen and Steps 2 and 3 are repeated.
5. Step 4 is repeated multiple times until all surface grains are considered. However, step 3 in not repeated for all of the surface grains. A method of choosing only the grains that initiate a crack that is likely to lead to failure is employed.
6. The life of the component is set equal to the minimum life of all of the cracks.

The details of the simulation are described below.

5.1 Crack Nucleation

A surface grain is simulated by generating grain diameter, d, the applied microstress, σ, the frictional stress needed to move dislocations, *k*, and the Schmid grain orientation factor, Ms from the appropriate distributions shown in Table 3 which are typical values for a high strength single phase alloy. These input values are the same as were used in earlier studies by the author. Thus, the results of the Monte Carlo FORTRAN software can be compared with the results of earlier studies. The microscopic stress intensity factor K_m is determined according to Eq. (25). If K_m is less than the critical stress intensity factor needed to overcome the grain boundary, K_{mc} , then the crack arrests at the grain boundary. The next surface grain is generated by repeating the process. If K_m is greater than K_{mc} , the number of cycles needed for crack nucleation is determined from one of the models presented in Section 3.2 and the crack will continue into the small crack phase.

Table 3: Input to the Monte Carlo Simulation

Variable	Description	Distribution Type	Distribution Parameters		Average	COV
C	Paris Law Coefficient	Lognormal	λ=-0.034	ζ=0.30	$4.4X10^{-9}\ MPa\sqrt{m}$	0.30
C'	CTOD Law Coefficient	Deterministic	N/A		0.10	N/A
d	Grain diameter	Lognormal	λ=-0.076	ζ=0.39	$55.8\mu m$	0.40
da	Small Crack Growth Interval	Deterministic	N/A		0.5	N/A
G	Bulk Shear Modulus	Deterministic	N/A		$76X10^{-3}\ MPa$	N/A
k	Frictional Strength	Weibull	η=1.12	ζ=3.7	$69MPa$	0.30
K_{crit}^{M}	Critical Microstructural Stress Intensity Factor	Deterministic	N/A		$769MPa\sqrt{m}$	N/A
M_S	Schmid Orientation Factor	Curve Fit			2.21	0.08
M_T	Taylor Orientation Factor	Curve Fit			3.07	0.13
n	Paris Law Exponent	Deterministic	N/A		3	N/A
W_S	Specific Fracture Energy	Deterministic	N/A		$440kN/m$	N/A
ν	Poisson's Ratio	Deterministic	N/A		0.3	N/A
σ	Applied Micro-stress	Normal	μ=1	σ=0.3	Variable*	0.30
*Note: The stress level of interest is a user input.						

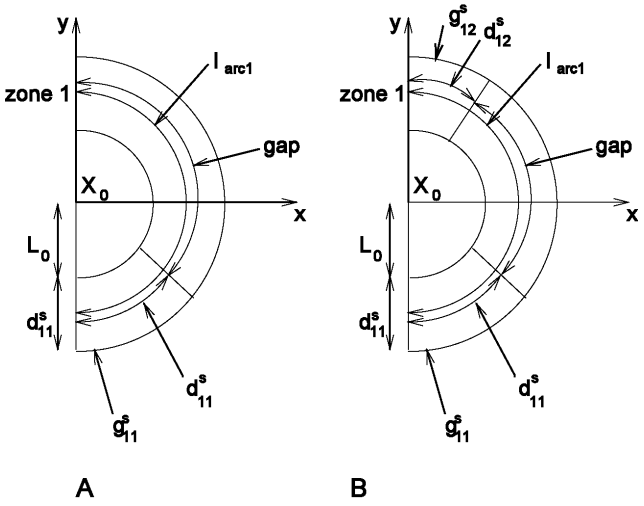

Figure 13: Representation of the simulated microstructure.

5.2 Small Crack Growth

In the small crack phase, the microstructure surrounding the crack nucleating grain is simulated by considering a crack nucleating at X_0 in Figure 13. Zone 1, directly in front of the crack, is simulated first. The properties d, σ, k, and M_s of grain g_{11}^s are generated using the appropriate distributions. The grain is a surface grain, therefore the Schmid factor orientation is assumed. The arc length l_{arc1} is determined by

$$l_{arc1} = \frac{\pi}{2}\left(\frac{L_0}{2} + \frac{d_{11}^s}{2}\right) = \frac{\pi}{4}\left(L_0 + d_{11}^s\right) \qquad (46)$$

If $d_{11}^s > l_{arc1}$ then the grain fills the zone and d_{11}^s is set equal to l_{arc1}. The properties of zone 1 are those generated for g_{11}^s.

If $d_{11}^s < l_{arc1}$ then the grain does not fill the space. A gap remains of size

$$gap = l_{arc1} - d_{11}^s \qquad (47)$$

The other surface grain g_{12}^s in zone 1 (see Figure 13B) is generated with the appropriate properties. The size of the grain d_{12}^s is compared with the gap.

If $d_{12}^s > gap$ then the grain fills the gap and d_{12}^s is set equal to the gap. The effective properties of the zone 1 are calculated as a weighted average with respect to the grain volume.

$$P_n = \frac{\sum_i^j P_i d_i^2}{\sum_i^j d_i^2} \qquad (48)$$

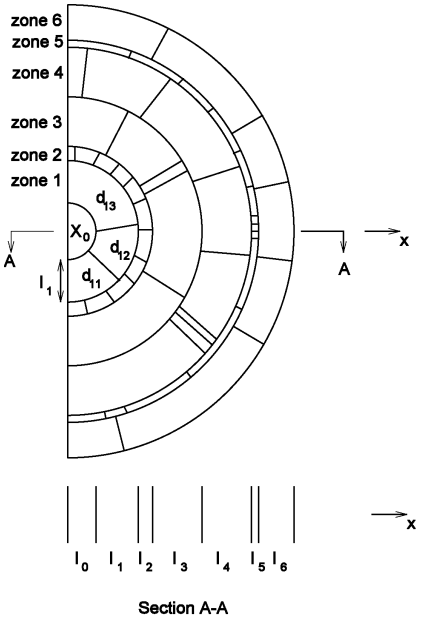

Figure 14: Microstructure created by the Monte Carlo simulation.

where P_n is the property or interest (grain orientation, microstructural stress, or fictional strength). If $d_{12}^s < gap$ then l_{arc1} is recalculated based on the average diameter of the two grains such that

$$l_{arc1} = \frac{\pi}{4}\left(L_0 + \frac{d_{11}^s + d_{12}^s}{2}\right) = \frac{\pi}{4}\left(L_0 + d_{1avg}^s\right) \qquad (49)$$

A gap remains of size

$$gap = l_{arc1} - d_{11}^s - d_{12}^2 \qquad (50)$$

An interior grain is now generated with the appropriate properties. The Taylor analysis is used for the orientation factor. If the grain fills the gap, then the grain size is set equal to the gap and the effective zone properties are calculated. If the grain does not fill the gap, then the arc length and the gap are recalculated and grains are generated until the gap is filled. The effective properties of the subsequent zones are generated using the same technique. The simulated microstructure can be represented by Figure 14.

Zones are generated until the effective material properties are within $\pm 10\%$ of the average material properties for three successive zones. Thus, the microstructure is generated until microstructural similitude is achieved. The number of zones and the total area of the zones are random and depend on the variation

of the microstructural properties. Microstructures with small variations will have a smaller region of dissimilitude than microstructures with large variations.

Once the microstructure surrounding the nucleating grain is simulated, the small crack growth is simulated. The equations governing small crack growth depend on the condition at the tip of the slip band. The theory and mathematical models used in the small crack growth analysis were outlined in the last bimonthly report. The following describes the flow of the Monte Carlo simulation.

5.2.1 *Propagated slip band.*

First, the propagated slip band phase is considered. The crack tip is at L_0 in Figure 14. The slip band tip is in zone 1.

If the effective microstructural stress, σ_{eff}, is greater than the effective frictional stress, k_{eff}, then the zone has yielded and the slip band tip has traversed to the next zone boundary. In this case, the propagated slip band phase requires zero cycles and the next phase of blocked slip band is considered.

If $\sigma_{eff} < k_{eff}$ then the slip band has not yet reached the next zone boundary and the position of the slip band tip is determined. An iterative technique is needed to solve for the location of the slip band tip because the equation describing its location is not closed form. Newton's method is used with the convergence criteria that successive values be within 0.1*da*, where *da* is the crack growth increment which is an input variable. (*da* must be some small fraction of the average grain diameter.) Once the location of the slip band tip has been determined, the crack tip opening displacement, ϕ_t, is evaluated. The number of cycles needed for the crack tip to traverse a distance *da* is calculated by

$$dN = \frac{C'\phi_t}{da} \tag{51}$$

where ϕ_t is the crack tip opening displacement. The new position of the crack tip is *a* + *da*. The process is repeated until the slip band tip reaches the next zone boundary. At this point, the blocked slip band phase begins.

5.2.2 *Blocked slip band.*

The crack tip is located at a determined form the above propagated slip band routine. The slip band tip is blocked at the zone boundary. The microscopic stress intensity factor K_m is calculated. If $K_m > K_{mc}$ then the slip band tip successfully penetrates the zone boundary. In this case, the blocked slip band phase requires zero cycles and the propagated slip band phase is considered for the next zone. If $K_m < K_{mc}$ then ϕ_t is calculated. The number of cycles needed for the crack tip to traverse a distance da is calculated using Eq. (51). The new position of the crack tip is $a + da$. The process is repeated until the slip band tip penetrates the zone boundary or the crack growth arrests.

The slip band tip will penetrate the zone boundary when $K_m > K_{mc}$. With each successive iteration, the crack tip grows *da* and K_m increases. However, as the crack tip approached the grain boundary, ϕ_t approaches zero. This causes *dN* to approach infinity in Eq. (51). Therefore, if $K_m < K_{mc}$ when the crack tip reaches the grain boundary, the crack growth arrest. In other word, if the crack tip reaches the zone boundary and the stress intensity factor is still less than critical, the crack stops growing.

If the crack growth arrest, the next surface grain is generated. If the crack growth does not arrest, the slip band tip successfully penetrates the zone boundary and the propagated slip band phase is considered for the next zone.

The crack continues to grow through propagated and blocked phases of successive zones until the crack is arrested or the slip band tip has reached the end of the microstructural dissimilitude region at which point the crack enters the long crack growth phase.

5.3 Long Crack Growth

Once the crack has reached the long crack growth stage there is no mechanism for blockage. The number of cycles spent in the long crack growth stage is calculated using Paris law.

6 Fatigue Life Predictions

6.1 Crack Nucleation

The crack nucleation model has previously been investigated by Tryon and Cruse [93, 94]. Tryon *et al*. [95] developed a first order reliability method (FORM) to investigate scatter in fatigue crack nucleation. The results of

the investigation are briefly presented here. The predicted shape of the crack nucleation life distribution was similar to the experimentally observed shapes found in the literature. The COV of crack nucleation life was predicted to increase as the applied load decreased and the COV was independent of the mean grain size. These predictions are in agreement with the experimental findings. Tryon and Cruse [94] use FORM to investigate the sensitivity of fatigue to the random variables and how the sensitivity changes with reliability level.

6.2 Small Crack Growth

Small crack growth behavior is modeled using the small crack growth phase of the Monte Carlo FORTRAN software. The results are determined using the parameters in Table 3 . These values are characteristic of a stainless steel. The results are compared with trends in the experimental data from the literature. The comparisons show that the small crack growth model is able to predict the significant aspects of small crack growth behavior.

One aspect of small crack growth behavior is that the average crack growth rate is much higher than what would be predicted based on long crack growth data and applied ΔK . Phillips and Newman [96] showed that, not only do small cracks grow much faster than ΔK equivalent long cracks, but that *da/dN* versus ΔK increases with applied stress. Thus, ΔK based similitude is not valid for small crack growth.

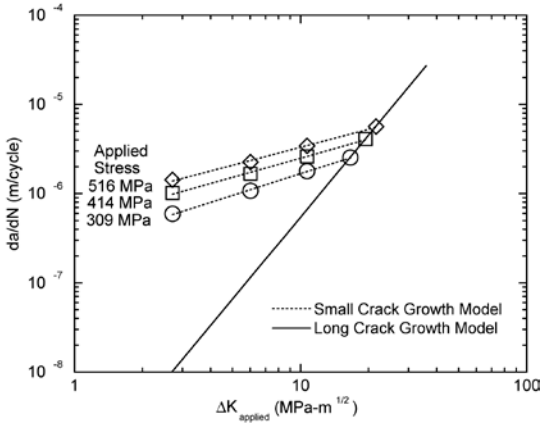

Figure 15: Predicted applied stress effect on crack growth rate.

Figure 15 shows the predicted average crack growth rate as a function of applied ΔK . The results compare favorably with experimental results of Phillips and Newman [97].

Another aspect of small crack growth behavior is that the mean crack growth rate for coarse grain microstructures is higher than the crack growth rate for fine grain microstructures of the same alloy [98]. This is in contrast to long crack growth rate behavior that shows that, in general, the crack growth rate for coarse grain microstructures is lower than fine grain microstructures. These observations are significant because the assumption has been made, based on long crack growth data, that the coarse grain materials produce better fatigue resistance. However, for cracking in service application, the small crack growth regime must be considered. The overall fatigue resistance may be driven by the small crack growth behavior [99].

Figure 16 shows the predicted average crack growth rate for two microstructures in which the average grain size has been changed. The figure shows that the crack growth rate is lower for the fine grain microstructure. In small cracks, the low growth rate for fine grain microstructures is attributed to the fact that there are more grain boundaries available to retard crack growth than what would be available over the same distance in a coarse microstructure. The difference in long crack growth rate for different grain size microstructures is attributed to two factors: closure and intergranular (grain boundary) cracking. The fine grain material has a smoother fracture surface allowing for less opposing crack face roughness induced closure. An element of intergranular cracking is observed as the plastic zone becomes large compared the grain size [100]. Intergranular crack growth rates are generally higher than transgranular [101]. The introduction of the intergranular cracking will take place at a lower ΔK for the fine grain material. A combination of less closure and more intergranular cracking causes a reduction in the overall fatigue resistance for the fine grain material.

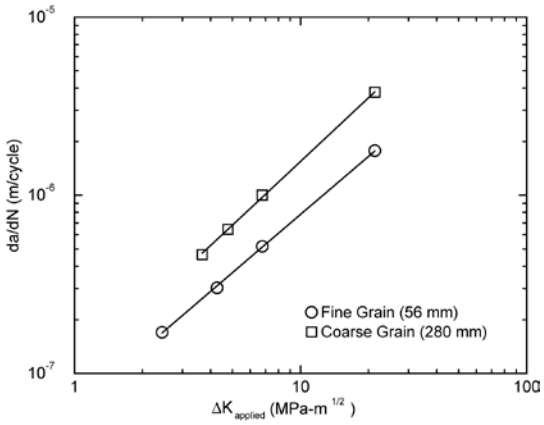

Figure 16: Predicted grain size effect on small crack growth rate.

Figure 17 shows the predicted crack growth rate as a function of crack length for 5 cracks that have successfully penetrated the first grain boundary. The crack growth rate seems to vary haphazardly as the crack interacts with the microstructure. Similar behavior has been observed experimentally by many investigators [102, 103]. The only obvious correlation that has been made between the crack growth rate and the microstructure is that the large jumps in

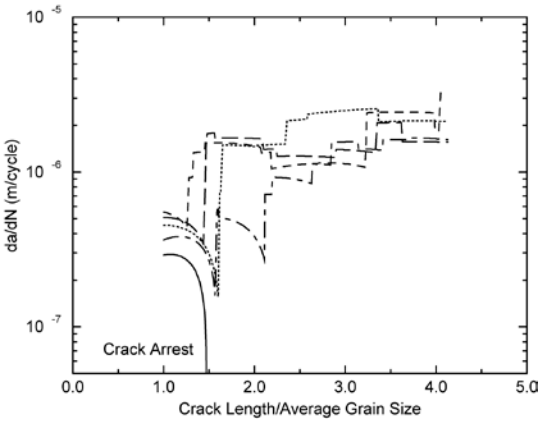

Figure 17: Predicted small crack growth behavior of five cracks.

crack growth rate can be associated with the crack tip nearing the grain boundary.

The small crack growth equations indicate that several factors govern the interaction between the crack growth rate and the microstructure.

1. The crack length.
2. The local effective resolved shear stress at the crack tip.
3. The local effective frictional stress at the crack tip.
4. The slip band length.
5. The effective resolved shear stress along the slip band.
6. The effective frictional stress along the slip band.
7. If the slip band tip is propagating or blocked.

To illustrate these interactions, consider the predicted small crack growth rate versus crack length curve for a single crack chosen at random shown in Figure 18. Grain boundaries are located at O, D, and F. The average frictional stress is 70 MPa. The average resolved shear stress is 41.4 MPa. The local effective properties are shown in the figure. The following list describes the conditions governing crack growth for the various regimes in Figure 18.

1. *Crack tip between O and A*. The crack tip is in zone 1. The slip band tip is propagating in zone 1.
2. *Crack tip between A and B*. The crack tip is in zone 1. The slip band tip is blocked at the boundary between zones 1 and 2.
3. *Crack tip between B and C*. The crack tip is in zone 1. The slip band tip is propagating in zone 2.
4. *Crack tip between C and D*. The crack tip is in zone 1. The slip band tip is blocked at the boundary between zones 2 and 3.
5. *Crack tip between D' and E*. The crack tip is in zone 2. The slip band tip is blocked at the boundary between zones 2 and 3.
6. *Crack tip between E' and F*. The crack tip is in zone 2. The slip band tip is blocked at the boundary between zones 3 and 4.
7. *Crack tip between F' and G*. The crack tip is in zone 3. The slip band tip is blocked at the boundary between zones 3 and 4.

As the crack grows the slip band becomes large and spans several grains. The crack continues to grow in such a manner until the effective properties of the material between the crack tip and the slip band tip approach the bulk properties.

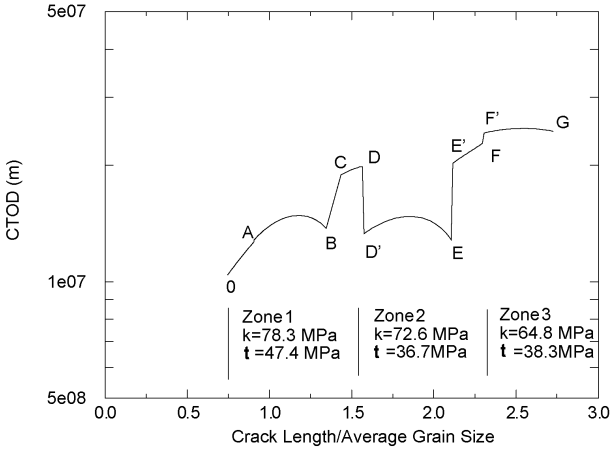

Figure 18: Predicted small crack growth behavior.

6.3 Predicted Total Fatigue Life of a Test Specimen

The most thorough investigation of the scatter in fatigue life available in the open literature is that of or most alloys Bastenaire [11]. Bastenaire performed an investigation of the scatter in fatigue life for five different grades of low alloy steel. Steels may nucleate cracks by mechanisms other than slip band cracking depending on the alloy composition and the impurities. However, the trend in the scatter in steel data has been observed in other metallic alloys [9]. Bastenaire performed rotating bending fatigue experiments for many stress levels for each grade of steel with several hundred specimens for each stress level.

Figure 20 shows the trends in the scatter exhibited in Bastenaire's data. (The curves are re-plotted from the data in Fig. 7 of Bastenaire) The general trend is that the COV (indicated by the slope of the curves) is fairy constant for applied stresses well above the fatigue limit (363-324 MPa). As the applied stress decreases, the COV starts to increase (304-285 MPa). As the applied stress approaches the fatigue limit, run-outs start to occur. The right tail of

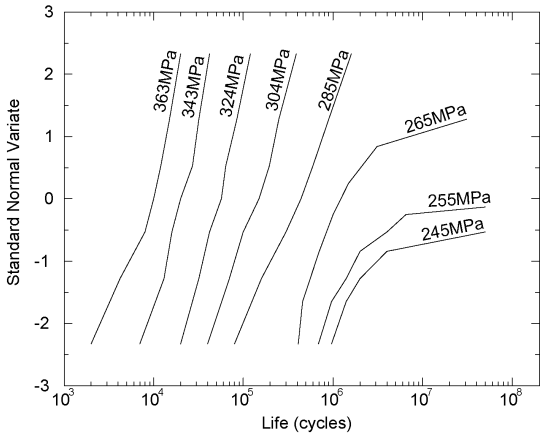

Figure 20: Fatigue life test data plotted on lognormal paper (data from Bastenaire (1972).

the distribution becomes heavy which causes a line through the data to bend to the right (265-245 MPa). If data plots as a non-straight line in Figure 20 the lognormal distribution is no longer valid. The 363 MPa data curves slightly to the left indicating the distribution has a short right tail and the data can also be fitted to the normal distribution. As the applied stress decreases, the curvature shifts to the right.

Comparison of Figure 20 with the results in Figure 19 shows that the model predicts all of the above trends observed in the experimental data.

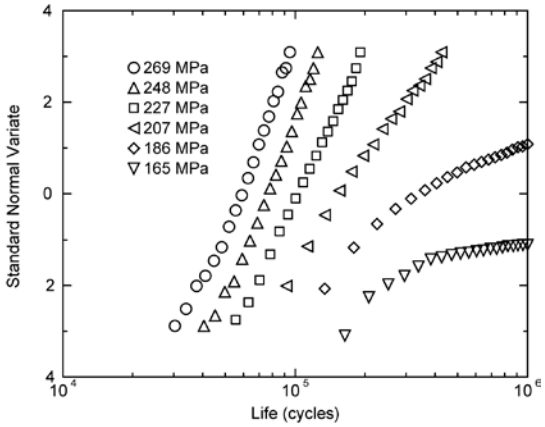

Figure 19: Predicted fatigue life distribution plotted on lognormal paper.

7 Conclusions

This paper showed the feasibility of probabilistic microstructural fatigue modeling. Information was found in the open literature on the mechanism that drive crack nucleation and small crack growth for many alloys. Damage accumulation models were developed that address the most important factors driving microstructural crack growth. The random variables that govern fatigue were estimated from empirical data and theoretical considerations. Statistical Volume Element FEM models based on Voronoi cells were able to accurately represent the local stress response. Simple closed-form equations were developed to approximations statistical volume element models based on the crystallographic anisotropy. A Monte Carlo simulation software was written which combined all of the above with the damage accumulation models to correctly predict:

- The shape of the crack nucleation life distribution
- Multiple cracks
- The applied global stress effects and the mean grain size effect on the COV of crack nucleation life.
- The applied global stress effects and the mean grain size effect on small crack growth rate.
- The variation in small crack growth rate.
- The shape of the total fatigue life distribution.
- The applied global stress effects on the shape of the total fatigue life distribution.

Acknowledgments – The author would like to the C. Chamis of NASA Glenn Research Center and J. Jira, A. Rosenberger and S. Russ of the Air Force Research Laboratory for their financial support. The author would also like to thank T. Cruse, Professor Emeritus of Vanderbilt University for his technical support.

1 Nisitani, H., and Takao, K-I. (1981) “Significance of Initiation, Propagation and Closure of Microcracks in High Cycle Fatigue of Ductile Metals”, Eng. Frac. Mech., Vol. 15, No. 3, pp. 445-456.
2 McDowell, D. L. (1997) "An Engineering Model for Propagation of Small Cracks in Fatigue", Eng. Frac. Mech., Vol. 56, pp. 357-377.
3 Taira S., Tanaka, K., Hoshina, M. (1979) “Grain Size Effect on Crack Nucleation and Growth in Long-Life Fatigue of Low-Carbon Steel”, *Fatigue Mechanisms* ,ASTM STP 675, Ed. Fong, J. T., pp. 135-173.
4 Floreen, S. (1980) “High Temperature Crack Growth Structure Property Relationships in Nickel Base Superalloys”, *Creep-Fatigue-Environment Interactions*, Ed., Pelloux, R., Slotoff, N., Metallurgical Soc., pp. 121-128.
5 Tokaji, K., Ogawa, T., Ohya, K. (1994) “The Effect of Grain Size on Small Fatigue Crack Growth in Pure Titanium”, Fatigue, Vol. 16, pp. 571-578.
6 Gayda, J., Miner, R. (1983a) “Fatigue Crack Initiation and Propagation in Several Nickel-Based Superalloys at 650C”, Int. J. Fat., Vol. 5, No. 3, pp. 135-143.
7 Lerch, B.(1982) “Microstructural Effects on the Room and Elevated Temperature Low Cycle Fatigue Behavior of Waspaloy”, NASA CR 165 497.
8 Lankford, J., and Davidson, D. L.(1986) “The Role of Metallurgical Factors in Controlling the Growth of Small Fatigue Cracks”, *Small Fatigue Cracks*, Ed., Ritchie, R. O. and Lankford, J., The Metallurgical Society, Warrendale, PA, pp. 51-71, 1986.
9 Sasaki, S., Ochi, Y., Ishii, A., Hirofumi, A. (1989) “Effects of Material Structures on Statistical Scatter in Initiation and Growth Lives of Surface Cracks and Failure Life in Fatigue”, JSME Inter. J., Series I, Vol. 32, No. 1, pp. 155-161 .
10 Bataille, A., Magnin, T. (1994) “Surface Damage Accumulation in Low Cycle Fatigue: Physical Analysis and Numerical Modelling”, Acta Metall. Mater., Vol. 42, No. 11, pp. 3817-3825.
11 Bastenaire, F. A., “New Method for the Statistical Evaluation of Constant Stress Amplitude Fatigue-Test Results”, Probabilistic Aspects of Fatigue, Ed., Heller, R. A., ASTM STP 511, pp. 3-28, 1972.
12 Goto, M.(1994) “Statistical Investigation of the Behaviour of Small Cracks and Fatigue Life in Carbon Steels with Different Ferrite Grain Sizes”, Fat. Frac. Engng. Mater. Struct., Vol. 17, No. 6, pp. 635-649.
13 Ishii, A., Ochi Y., Sasaki, S. K. and Nakamura, H. (1991) “Effect of Microstructure on Statistical Scatter of Crack Initiation and Growth Lives in NiCrMoV Cast Steel”, J. Soc. of Mat. Sci., Japan/Zairyo, Vol. 40, No. 452, pp. 568-574.
14 Fu-Ze, Z.(1991) “The Fatigue Scatter Factors and Reduction Factors in the Design of Aircraft and Helicopter's Structural Lives,” 47th Annual Forum Proc. of the American Helicopter Society, Vol. 911984, pp. 173-178.
15 Goto, M.(1991) “Statistical Investigation of the Behaviour of Microcracks in Carbon Steel”, Fat. Frac. Engng. Mater. Struct., Vol. 14, No. 8, pp. 833-845.
16 Sasaki, S. K., Ochi, Y., and Ishii, A. (1987) “Statistical Investigation of Surface Fatigue Cracks in Large-sized Turbine Rotor Shaft Steel”, Eng. Frac. Mech., Vol. 28, No. 5/6, pp. 761-772.
17 Dieter, G. E.(1986) *Mechanical Metallurgy*, McGraw-Hill, Third Edition.
18 Gokhale, A. B., Rhimes, F. N.(1983) “Effect of Grain Volume Distribution on the Plastic Properties of High Purity Aluminum”, {\it Microstructural Science}, Vol. 11, Ed., DeHoff, R., Braum, J., McCall, J., Elsevier, pp. 3-11.
19 Halford, G. R. (1991) “Evolution of Creep-Fatigue Life Prediction Models”, Creep-Fatigue Interactions at High Temperatures, AD-Vol. 21, Ed., Haritos, G. K., Ochoa, O. O., ASME, pp. 43-57.
20 Schijve, J. (1994) “Fatigue Predictions and Scatter”, Fat. Frac. Eng. Mat. Struct., Vol. 17, No. 4, pp. 381-396.
21 Little, R. E., and Jebe, E. H. (1975) *Statistical Design of Fatigue Experiments*, Applied Science Publ., Essex U.K.
22 Axelrad, D. R. (1980) “The Mechanics of Discrete Media”, *Continuum Models of Discrete Systems (CMDS3)*, Ed., Kroner, E., Anthony, K.-H., Univ. Waterloo, pp. 3-34.
23 Haritos, G. K., Hager, A. K., Salkind, M. J., Wang, A. S. D. (1988) “Mesomechanics: The Microstructure-Mechanics Connection”, Int. J. Sol. Struct., Vol. 24, No. 11, pp. 1081-1096.
24 Peterson, R. E.(1939) “Methods of Correlating Data from Fatigue Test of Stress Concentration Specimens,” *Contributions to the Mechanics of Solids*, Macmillan, pp. 179-183.

25 Fong, J. T.(1979) “Statistical Aspects of Fatigue at Microscopic, Specimen, and Component Levels,” *Fatigue Mechanisms, ASTM STP 675*, pp. 729-758.
26 Smith, R. A.(1983) “Short Fatigue Cracks”, *Fatigue Mechanism: Quantitative Measurements of Physical Damage*, STP 811 Ed. Lankford, J., Davidson D. L., Morris, W. L., Wei, R. P., ASTM, pp. 264-297.
27 Ghosh, S., Moorthy, S. (1995) "Elastic-plastic analysis of arbitrary heterogeneous materials with Voronoi Cell finite element method", Computer Methods in Applied Mech. Engrg., 121, pp. 373-409.
28 Fine, M. E. and Kwon, I. B. (1986) “Fatigue Crack Initiation Along Slip Bands”, *Small Fatigue Cracks*, Ed., Ritchie, R. O. and Lankford, J., The Metallurgical Society, Warrendale, PA, pp. 29-40.
29 Laird, C. (1979) “Mechanisms and Theories of Fatigue”, *Fatigue and Microstructure*, ASM, Metals Park, Ohio, pp. 149-203.
30 Kuhlmann-Wilsdorf, D. (1977) “Dislocation Behavior in Fatigue”, Mat. Sci. Eng., Vol. 27, pp. 137-156.
31 Forsyth, P. (1969) *The Physical Basis of Metal Fatigue*, American Elsevier Publ., New York.
32 Brown, L. M. (1977) “Dislocation Substructure and the Initiation of Cracks by Fatigue”, Metal Sci., Aug./Sept., pp. 315-320.
33 Grobstein, L. L., Sivashankaran, S., Welsch, G., Panigrahi, N., McGervery, J. D., Blue, W. (1977) “Fatigue Damage Accumulation in Nickel Prior to Crack Initiation”, Mat. Sci. Eng., Vol. A138, pp. 191-203.
34 Tanaka, K., Mura, T. (1981) "A Dislocation Model for Fatigue Crack Initiation", *ASME J. Appl. Mech.*, Vol. 48, pp. 97-103.
35 Laird, C., Duquette, D. J. (1972) “Mechanisms of Fatigue Nucleation”, Proceedings, Inter. Corrosion Fatigue Conference, Ed., Devereux, 0., McEvely, Steable, R. W, pp. 88-117.
36 Laird, C. (1977) “Recent Advances in Understanding the Cyclic Deformation of Metals and Solid Solutions”, *Work Hardening in Tension and Fatigue*, The Metallurgical Society, New York, pp. 150-176.
37 Chan, K. S., Lankford, J. (1983) “A Crack Tip Strain Model for the Growth of Small Fatigue Cracks,” Scripta Metall., Vol. 17, pp. 529-532, 1983.
38 Newman, J. C., Swain, M. H., Phillips, E. P. (1986) “An Assessment of the Small-Crack Effect for 2024-T3 Aluminum Alloy”, *Small Fatigue Cracks*, Ed., Ritchie, R. O. and Lankford, J., The Metallurgical Society, Warrendale, PA, pp. 427-452.
39 Grosskreutz. J. C. (1971) “The Mechanism of Metal Fatigue”, Physica Status Solidi, Vol. 47b, pp. 359-396.
40 Sasaki, S., Ochi, Y. (1979) “Some Experimental Studies of Fatigue Slip Bands and Persistent Slip Bands During Fatigue Process of Low-Carbon Steel”, Eng. Frac. Mech., Vol. 12, pp. 531-540.
41 Head, A. K., and Louat, N. (1955) “The Distribution of Dislocations in Linear Arrays,” Aus. J. Phys., Vol. 8, pp. 1-7.
42 Bilby, B. A., Eshelby, J. D.(1968) “Dislocations and the Theory of Fracture,” *Fracture*, Vol. 1, ed. H. Liebowitz, pp. 99-182.
43 Chang, R., Morris, W. L., Buck, O. (1979) “Fatigue Crack Nucleation at Intermetallic Particles in Alloys - A Dislocation Pile-Up Model,” Scripta Metall., vol. 13, pp. 191-194.
44 Mura, T., Tanaka, K. (1981) "A Dislocation Dipole Models for Fatigue Crack Initiation", Mechanics of Fatigue, AMD Vol. 47, ASME, pp. 111-132.
45 Kato, M., and Mori, T. (1992) “Statistical Consideration of Fatigue Damage Accumulation”, Mech. Mat., 13, pp. 155-163.
46 Cooper, C. V., Fine, M. E. (1984) “Coffin-Manson Relation for Fatigue Crack Initiation,” Scripta Metall., Vol. 18, pp. 593-595.
47 Muskhelishvili, N. I. (1977) *Singular Integral Equations*, Noordhoff Inter.
48 Davidson, D. L. (1988) “Small and Large Fatigue Cracks in Aluminum Alloys”, Acta Metall., Vol. 38, No. 8, pp. 2275-2282.
49 Mura, T., and Nakasone, Y. (1990) “A Theory of Fatigue Crack Initiation in Solids”, J. Appl. Mech., 57, pp. 1-6.
50 Venkatraman, G., Chung, Y-W., Nakasone, Y., and Mura, T. (1990) “Free Energy Formulation of Fatigue Crack Initiation Along Persistent Slip Bands: Calculation of S-N Curves and Crack Depths”, Acta Metall. Mater., 38, pp. 31-40.
51 Laird,, D., Smith G. C. (1962) “Crack Propagation in High Stress Fatigue”, Phil. Mag., Vol. 7 PP. 847-857.
52 Weertman, J. (1979) “Fatigue Crack Propagation Theories”, *Fatigue and Microstructure*, ASM, Metals Park, Ohio, pp. 279-206.
53 Kikukawa, M., Jono, M., Adachi, M. (1979) “Direct Observation and Mechanics of Fatigue Crack Propagation”,

Proceedings of an ASTM-NBS-NSF symposium, Ed. Fong, J. T., ASTM STP 675, pp. 234-253.
54 Hicks, M. A., Brown, C. W. (1984) "A Comparison of Short Crack Growth Behaviour in Engineering Alloys", *Fatigue 84*, Engineering Materials Advisory Services Ltd., England, pp. 1337-1347.
55 Hudak, S. J., Chan, K. S. (1986) "In Search of a Driving Force to Characterize the Kinetics of Small Crack Growth", *Small Fatigue Cracks*, Ed., Ritchie, R. O. and Lankford, J., The Metallurgical Society, Warrendale, PA, pp. 379-406.
56 Tanaka K., Kinefuchi, M., and Yokomaku, T.(1992) "Modelling of Statistical Characteristics of the Propagation of Small Fatigue Cracks", Short Fatigue Cracks, Eds. Miller, K. J., and de los Rios, E. R., ESIS 13, Mechanical Engineering Publications, London, pp. 351-368.
57 Ewalds, H. L., Wanhill, R. J. H. (1991) *Fracture Mechanics*, Edward Arnold Publ., New York.
58 Donahue, R. J., Clark, H. M., Atanmo, P., Kumble, R., McEvily, A. J. (1972) Inter. J. of Frac. Mech., Vol. 8, pp. 209.
59 McEvily, A. J. (1974) *Microstructure and Design of Alloys, Vol. 2*, Inst. of Metals, pp. 204, 1974.
60 Kikukawa, M., Jono, M., Tanaka, K.(1976) "Fatigue Crack Closure Behavior at Low stress Intensity Lever", Proc. of ASM Mech. Behavior of Mat., Boston, pp. 716-720.
61 Hobson, P. D. (1982) "The Formulation of a Crack Growth Equation for Short Cracks," Fat. Engng. Mater. Struct., Vol. 5, pp. 323-327.
62 Chan, K. S., Lankford, J. (1988) "The Role of Microstructural Dissimilitude in Fatigue and Fracture of Small Cracks," Acta Metall., Vol. 36, No. 1, pp. 193-206.
63 Gerberich, W. W., Moody, N. R. (1979) "A Review of Fatigue Fracture Topology Effects on Threshold and Growth Mechanisms,", *Fatigue Mechanisms, ASTM STP 675*, pp. 292-341.
64 Dugdale, D. S.(1960) "Yielding of Steel Sheets Containing Slits," J. Mech. Phys. Sol., Vol. 8, pp. 100-104.
65 Weertman, J. (1966) "Rate of Growth of Fatigue Cracks Calculations from the Theory of Infinitesimal Dislocations Distributed on a Plane," J. Frac. Mechs., Vol. 2, pp. 460-467.
66 Bilby, B. A., Cottrell, A. H., Swinden, K. H. (1963) "The Spread of Plastic Yield from a Notch," Proc. Roy. Soc., Vol. A272, pp. 304-314.
67 Weertman, J. (1984) "Crack Tip Stress Intensity Factor of the Double Slip Plane Crack Model: Short Cracks and Short Short-cracks," Int. J. Frac., Vol. 26, pp. 31-42.
68 Taira, S., Tanaka, K., Nakai, Y.(1978) "A Model of Crack Tip Slip Band Blocked by Grain Boundary," Mech. Res. Comm., Vol. 5, No. 6, pp. 375-381.
69 Tanaka, K., Akiniwa, Y., Nakia, Y., Wei, R. P. (1986) "Modeling of Small Fatigue Crack Growth Interacting with Grain Boundary," Engng. Frac. Mechs., Vol. 24, No. 6, pp. 803-819.
70 Morris, W. L., James, M. R.,, Buck, O. (1983) "A Simple Model of Stress Intensity Range Threshold and Crack Closure Stress," Engng. Frac. Mechs., Vol. 18, pp. 871-877.
71 de los Rios, E. R., Tang, Z., Miller, K. J. (1984) "Short Crack Fatigue Behavior in a Medium Carbon Steel," Fat. Engng. Mat. Struct., Vol. 7, pp. 97-108.
72 Navarro, A., de los Rios, E. R. (1988) "A Microstructurally Short Fatigue Crack Growth Equation," Fat. Frac. Engng. Mater. Struct., Vol. 11, No. 5, pp. 383-396.
73 Newby, M. J.(1987) "Markov Models for Fatigue Crack Growth", Eng. Frac. Mech., Vol. 27, No. 4, pp. 477-482.
74 Yang, J. N., Salivar, G. C., Annis, C. G. (1982) Statistics of Crack Growth in Engine Materials - Volume 1: Constant Amplitude Fatigue Crack Growth at Elevated Temperatures, AFWAL-TR-82-4040.
75 Morris, W. L., James, M. R.,, Buck, O. (1980) "Computer Simulation of Fatigue Crack Initiation," Engng. Frac. Mechs., Vol. 13, pp. 213-221.
76 Smith, C. S.(1981) A Search for Structure, MIT Press, Cambridge.
77 Kurtz, S. K., Carpay, F. M. A.(1980) "Microstructure and Normal Grain Growth in Metals and Ceramics. Part I. Theory", J. Appl. Phys., Vol. 51, No. 11, pp. 5725-5744.
78 Kumar, S., Kurtz, S. K., Banavar, J. R., Sharma, M. G. (1992) "Properties of a Three-Dimensional Poisson-Voronoi Tessellation: A Monte Carlo Study", *Journal of Statistical Physics*, Vol. 67, Nos. 3/4, pp. 523-551.
79 Ang, A. H.-S., Tang, W. H.(1975) Probability Concepts in Engineering Planning and Design, Vol. 1, John Wiley and Sons, New York.
80 Barrett, C. S. (1952) Structure Of Metals, McGraw-Hill Book Company, Inc., Second edition.
81 Taylor, G. I.(1938) "Plastic Deformation in Metals", J. Inst. Metals, Vol. 62, pp. 307-24.
82 Bishop, J. F. W., Hill, R., Phil. Mag., Vol. 42, pp. 1298-1307, 1951.

83 Chin, G. Y., Mammel, W. L.(1967) “Computer Solution of the Taylor Analysis for Axisymmetric Flow”, Trans. Metall. Soc., Vol. 239, pp. 1400-1405.
84 Davidson, D. L., Chan, K. S.(1989) “The Crystallography Of Fatigue Crack Initiation In Coarse Grained Astroloy At 20 C”, Acta Metall., Vol. 37, No. 4, pp. 1089-1097.
85 Ono, N., Kimura, K., Watanabe, T. (1999) “Monte Carlo Simulation of Grain Growth with the Fill Spectra of Grain Orientation and Grain Boundary Energy”, Acta Mater., Vol. 47, pp. 1007-1017.
86 Backofen, W. A.(1972) Deformation Processing, Addison-Wesley, pp. 72-82.}
87 Tanaka, T., Kosugi, M.(1988) “Crystallographic Study of the Fatigue Crack Nucleation Mechanism in Pure Iron”, Basic Questions in Fatigue, Vol. 1, ASTM STP 924, pp. 98-119.
88 Backofen, W. A.(1972) Deformation Processing, Addison-Wesley, pp. 72-82.}
89 Sun, Z., de los Rios, E. R., Miller, K. J.,(1991) “Modelling Small fatigue Cracks Interacting with Grain Boundaries”, Fat. Frac. Engng. Mater. Struct., Vol 14. No. 2/3, pp. 277-291.
90 James, M. R., Morris, W. L.(1986) “The Effect of Microplastic Surface Deformation on the Growth of Small Cracks”, Small Fatigue Cracks, Ed., Ritchie, R. O. and Lankford, J., The Metallurgical Society, Warrendale, PA, pp. 145-156.
91 Barenblatt, G. I.(1987) “On a Model of Small Fatigue Cracks”, Eng. Frac. Mech., Vol. 28, No. 5/6, pp. 623-626.
92 Zhao, Y., Tryon, R. G.(2002) “Automatic Simulation of Polycrystalline Metallic Materials”, ISSAT International Conference on Reliability and Quality in Design, Anaheim, CA., 7-9 Aug, 2002, pp. 6-10.
93 Tryon, R. G., Cruse T. A. (1997) "Probabilistic Mesomechanical Fatigue Crack Nucleation Model", *ASME J. Engrg .Mat. Tech*, Vol. 119, pp. 257-267.
94 Tryon, R. G., Cruse, T. A. (1998) "A Reliability-Based Model to Predict Scatter in Fatigue Crack Nucleation Life", Fat. Frac. Eng. Mat. Str., Vol. 21, pp. 257-267.
95 Tryon, R. G., Cruse, T. A., Mahadevan, S. (1996) “Development of a Reliability-Based Fatigue Life Model for Gas Turbine Engine Structures”, Engr. Frac. Mech., Vol. 53, No. 3, pp. 807-828.
96 Phillips, E. P., Newman, J. C.(1989) “Impact of Small-Crack Effects on Design-Life Calculations”, Experimental Mech., Vol. 29, No. 2, pp. 221-225.
97 Phillips, E. P., Newman, J. C.(1989) “Impact of Small-Crack Effects on Design-Life Calculations”, Experimental Mech., Vol. 29, No. 2, pp. 221-225.
98 Gerdes, C., Gyser, A., Lutjering, G.(1984) “Propagation of Small Surface Cracks in Ti-Alloys”, Fatigue Crack Growth Threshold Concepts, Ed. Davidson, D. L., Suresh, S., AIME, Warrendale, PA., pp. 465-478.
99 Brown, C. W., King, J. E.(1986) “The relevance of microstructural Influenced in the Short Crack Regime to Overall Fatigue Resistance”, Small Fatigue Cracks, Ed., Ritchie, R. O. and Lankford, J., The Metallurgical Society, Warrendale, PA, pp. 73-95.
100 Gayda, J., Miner, R. V.(1983b) “The Effect of Microstructure on 650C Fatigue Crack Growth in P/M Astroloy”, Metall. Trans. A, Vol. 14A, pp. 2301-2308.
101 Lerch B. A., Jayaraman, K., Antolovich, S. D.(1984) “A Study of Fatigue Damage Mechanisms in Waspaloy for 25 to 800C”, Mat. Sci. Eng., Vol. 66, pp. 151-166.
102 Tokaji, K., Ogawa, T.(1992) “The Growth Behaviour of Microstructurally Small Fatigue Cracks in Metals”, Short Fatigue Cracks, Eds. Miller, K. J., and de los Rios, E. R., ESIS 13, Mechanical Engineering Publications, London, pp. 85-99.
103 Reed, P. A., King, J. E., “Comparison of Long and Short Crack Growth in Polycrystalline and Single Crystal Forms of Udimet 720”, Short Fatigue Cracks, Eds. Miller, K. J., and de los Rios, E. R., ESIS 13, Mechanical Engineering Publications, London, pp. 153-168, 1992.